Nanosized Glutathione- and Enzyme-Sensitive Carriers Based on Hyaluronic Acid for Hydrophilic Payload Delivery

Suresh Ajmeera[a,b], *Ines Tejeda*[c], *Alessia Pancaro*[a,b,d], *Elien Derveaux*[e], *Annelies Bronckaers*[f], *Peter Adriaensens*[e], *Inge Nelissen*[d], *Karen Smeets*[c], *Anitha Ethirajan*[a,b*]

[a] Hasselt University, Institute for Materials Research (imo-imomec), Nanobiophysics and Soft Matter Interfaces (NSI) group, Martelarenlaan 42, B-3500 Hasselt, Belgium

[b] imec, imo-imomec, Wetenschapspark 1, B-3590 Diepenbeek, Belgium

[c] Hasselt University, Toxicology Lab, Centre for Environmental Sciences (CMK), Agoralaan D, B-3590 Diepenbeek, Belgium

[d] Flemish Institute for Technological Research (VITO), Environmental Intelligence Unit, Boeretang 200, 2400 Mol, Belgium

[e] Hasselt University, Institute for Materials Research (imo-imomec), Applied and Analytical Chemistry, NMR group, Agoralaan D, B-3590 Diepenbeek, Belgium

[f] Hasselt University, Biomedical Research Institute (BIOMED), Laboratory of ischemic stroke, angiogenesis and stem cells (LISSA), Agoralaan C, B-3590 Diepenbeek, Belgium

*Email: anitha.ethirajan@uhasselt.be

KEYWORDS: Redox-responsive nanocarriers, Dual-stimuli, Biocompatible, Biodegradable, Hydrophilic drug delivery, life-threatening ailments.

ABSTRACT

Redox-responsive nanocarriers (NCs) for drug delivery have gained continuous interest in precision medicine. However, the complexity of redox balance between the different oxidative (e.g., reactive oxygen species) and anti-oxidative (e.g., glutathione, GSH) species in various pathological conditions (e.g., tumor, inflammation) makes site-specific payload release challenging. Moreover, hydrophilic bio-active substances undergo rapid clearance by the reticuloendothelial system. These obstacles underscore the necessity for novel strategies to enhance the precision and safety of redox-responsive NCs for hydrophilic payload delivery.

Herein, we present a simple and efficient approach to fabricate hydrophilic cargo-loaded dual-responsive hyaluronic acid (HA) based NCs using inverse miniemulsion interfacial cross-linking chemistry. By simply combining HA and bis (4-hydroxyphenyl) disulfide (HPD) as separate precursors in the formulation (i.e., without the need for prior chemical conjugation of HA and HPD), biopolymer-based NCs sensitive to hyaluronidase and GSH are achieved. A fluorescent dye, sulforhodamine B and an anticancer drug, doxorubicin (DOX), were used as payloads. The characterization of NCs using dynamic light scattering and transmission electron microscopy exhibited < 200 nm size with a narrow distribution and a core-shell nanocapsule morphology. We successfully obtained NCs with an encapsulation efficiency > 90 %, and the release studies showed that the encapsulated payloads were liberated in a sustained and controlled manner upon exposure to both GSH and enzymatic triggers at varying concentrations. In the *in vitro* studies, no noticeable cytotoxicity was seen when human-derived dental pulp stem cells and lung cancer cells (A549) were exposed to NCs (up to 100 μg/ml), and a decrease in cell viability of A549 cells was observed

with increasing concentration of DOX-loaded NCs. Moreover, the NCs were internalized in the cells after 24 h of exposure. These dual-responsive biocompatible and biodegradable NCs have an enormous scope in the delivery of hydrophilic therapeutics to treat various life-threatening ailments.

INTRODUCTION

Redox-responsive nanocarriers (NCs) represent a promising class of drug delivery systems designed to exploit the unique intracellular pathological redox environment for targeted therapy, while maintaining stability in physiological conditions.[1] By utilizing the intracellular pathological elevated levels of ROS or GSH, these NCs aim to achieve selective drug release, thereby minimizing systemic toxicity and enhancing therapeutic efficacy.[2] However, several challenges impede their development and application. The variability in redox conditions at the intracellular diseased sites makes it challenging to design universally effective NCs.[3] Additionally, the therapeutic administration of hydrophilic bio-active components such as drugs, probes, inhibitors, growth factors, and genetic materials faces significant obstacles due to their rapid degradation, systemic clearance in physiological environments, short half-life, and limited transmembrane permeability.[4] Ensuring stability in the physiological environment while preventing premature drug release, specifically for hydrophilic payloads, requires sophisticated NC design strategies. Encapsulation strategies such as lipid nanoparticles or nanomaterials still suffer from low drug loading efficiency and controlled release kinetics.[5] Moreover, the biocompatibility and potential toxicity of materials used are still major concerns that can limit NCs in clinical usage. Therefore, there is a need for innovative yet simple NC design that is biocompatible, can encapsulate hydrophilic payloads, and deliver the payload specifically in the intracellular pathological environments.

Hyaluronic acid (HA) is a linear hydrophilic biodegradable polysaccharide composed of repeating disaccharide units of D-glucuronic acid and N-acetyl glucosamine linked by β (1,4) and β (1,3) glycosidic bonds. It is a non-antigenic, non-toxic, and non-immunotoxic naturally occurring polysaccharide with high bio-reconcilability.[6] HA can generally affect cellular processes such as differentiation, proliferation, growth, molecular recognition, and physiological processes like lubrication, hydration balance, matrix construction, and steric interactions.[7] It can be produced on a large scale from animal tissues, by bacterial synthesis, or via cell-free generation.[7] Due to its biological characteristics and abundance, HA has been vastly used in many drug delivery applications such as protein-HA conjugate for ocular disease, HA hydrogels as bioreactors, tissue-engineering scaffolds and diagnostics, and HA nanogels to combat bacterial infections.[7] In recent decades, the strong affinity for the CD44 receptor and receptor for hyaluronan-mediated motility has drawn enormous attention to fabricating NCs to treat different cancer types and inflammatory diseases.[8, 9] These conditions are characterized by overexpression of the CD44 receptor and dysregulated redox homeostasis.[10] Moreover, the hyaluronidase (HAase) enzyme's capability to disintegrate HA has been utilized to develop multi-stimuli responsive NCs by combining it with redox-sensitive moieties.[11] In general, the stimuli-sensitive HA-based NCs for hydrophilic payload delivery can be prepared by covalent conjugation,[12] ionic gelation with cationic polymers,[13] or microfluidic flow assembly method.[14, 15] However, the chemical modifications to achieve redox-responsiveness disrupt the innate biopolymer activity.[16] The alteration in the HA can lose its affinity towards the CD44 receptor, which is essential for the internalization of NCs.[16] Chiesa *et al.*[17] proposed a microfluidic self-assembly approach without modifying HA and successfully achieved protein-loaded nanoparticles and CD44 internalization, but still suffered from low encapsulation efficiency and pre-mature release at physiological conditions. Another study by

Oommen *et al.*[18] synthesized a prodrug with HA (high weight average molecular weight, 150 kDa) that retained CD44 affinity, but possessed low loading content and a dose-dependent decrease in cell viability. However, despite the excellent benefits of prodrugs, tuning of drug loading capacity is laborious and time consuming. Additionally, the covalent conjugation of the drugs to polymers may compromise the drug's and polymer's innate biological activity, and higher amounts of polymers may lead to potential toxicity.[19] Attempts have been made to design chemically crosslinked multi-stimuli (GSH/HAase/pH) responsive HA-decorated silica-based NCs to deliver the doxorubicin, anticancer drug.[20, 21] However, the physical adsorption of the drug in the pores of silica led to a lower loading content, and the chemical modifications of HA decreased the biocompatibility of these NCs over time. These limitations highlight the need for a simple and effective approach to fabricating responsive HA-based NCs with an aqueous core for hydrophilic payload delivery without any chemical alterations.

In this regard, the miniemulsion technique offers flexibility in design of nanocarriers with tunable physicochemical properties using preformed polymers as well as in-situ polymerization using suitable precursors.[22-26] By using inverse (oil in water) miniemulsion (IME) method, NCs with aqueous core can be developed for hydrophilic payload delivery. The IME method has been proven to synthesize NCs with various chemical compositions, while having high encapsulation efficiency and therapeutic efficacy.[27-29] The IME method consists of two phases: an aqueous phase consisting of monomers/polymers and a payload and an oil phase containing a non-polar solvent in which an emulsifier is dissolved. By applying high shear forces, nano-sized droplets can be formed, which further can be interfacially crosslinked to form NCs. These NCs gained enormous attention due to their capability to encapsulate high payloads and they can be used to deliver hydrophilic bioactive

compounds like small-molecule drugs or proteins in a solubilized form, protecting them from premature release.[29, 30]

In this work, we demonstrate the fabrication of sulforhodamine B (SRB, a hydrophilic surrogate compound with fluorescent properties)/ DOX-loaded GSH- and HAase-responsive hyaluronic acid (HA) and bis (4-hydroxyphenyl) disulfide (HPD) NCs using IME interfacial cross-linking chemistry.[25] For physical characterization of NCs we used dynamic light scattering (DLS) and transmission electron microscopy (TEM). The chemical composition of NCs was confirmed through attenuated total reflectance – Fourier transform infrared spectroscopy and nuclear magnetic resonance (liquid and solid state) spectroscopy. Release studies were performed in the presence of both HAase and GSH triggers at physiological conditions. The various concentrations of GSH and HAase were chosen to determine the optimal range where the NCs start responding to stimuli. It has been reported that GSH levels are 10 times higher in most tumor cells and inflamed/injured sites (1 – 15 mM) compared to healthy cells, 0.5 – 20 μM in extracellular and 0.5 – 3 mM in intracellular environments.[31, 32] Moreover, HAase overexpression in cancer cells and its role in metastasis[33, 34] and tissue regeneration[35] have been well established. Therefore, these endogenous biological cues have been exploited in this study for potential therapeutic drug delivery applications. Human primary-derived dental pulp stem cells (DPSCs) and A549 lung carcinoma cells, both expressing CD44 receptors, were used for cell viability and cellular uptake studies.[36, 37]

EXPERIMENTAL SECTION

Materials

Sodium Hyaluronate (Na-HA) (M_n = 8 – 15 kDa) was purchased from Contipro (Czech Republic). Dowex ® 50WX8 hydrogen form (strongly acidic, 50-100 mesh), Toluene diisocyanate (TDI), and Sodium dodecyl sulfate (SDS) were bought from Sigma-Aldrich (Belgium). Sodium hydroxide

(NaOH), Sodium chloride (NaCl), Potassium chloride (KCl), Dimethyl sulfoxide (DMSO, 99.7%), F-12K Medium (Kaighn's Modification of Ham's F-12 Medium), Dulbecco's modified eagles medium: nutrient mixture F12 (DMEM/F-12) without phenol red, and Hoechst 33342 were all purchased from Fischer Scientific (Belgium). Bis(4-hydroxyphenyl) disulfide (HPD) (>98%) and Doxorubicin hydrochloride (DOX) (>95%) were supplied by TCI Europe NV (Belgium). Triethylamine (TEA) and Sulforhodamine B sodium salt (SRB) (>98%) were purchased from Arcos Organics (Belgium). Alamar Blue, CellMask green actin tracking stain, and 4',6-Diamidino-2-Phenylindole (DAPI) were bought from Invitrogen (Oregon, USA). Dulbecco's modified eagles medium (∝-MEM and DMEM (without phenol red)), Phosphate buffered saline (PBS, $+Ca^{+2}$ and $+Mg^{+2}$), and Dulbecco's phosphate-buffered saline (DPBS, $-Ca^{+2}$ and $-Mg^{+2}$) were purchased from Gibco (Belgium). Wheat Germ Agglutinin (WGA)-Alexa Fluor 488 was purchased from VWR (Belgium). Paraformaldehyde (PFA), Fetal bovine serum (FBS), Penicillin/Streptomycin, and L-glutamine were bought from Sigma-Aldrich (Germany). Hypermer B246 was received from Croda Europe Ltd. (United Kingdom). Cyclohexane (>99.7%) was bought from Honeywell (Belgium). The deuterated solvents DMSO-d6, $CDCL_3$, and D_2O for NMR analysis were purchased from Fischer Scientific (Belgium). All chemicals were used as received. Milli Q (MQ) water was made using the Arium® Pro ultrapure water system (Sartorius Stedim Biotech, Germany).

Nanocarrier synthesis

Firstly, the sodium hyaluronate (Na-HA) was converted to acid form (HA-COOH) based on the procedure of Huerta-Angeles *et al.* with slight modifications.[38] Briefly, 200 mg of Na-HA was dissolved in 3 ml of MQ water in a single neck round bottom flask. Excess Dowex resin was added to this solution and stirred for 10 – 12 hours (h). The resultant mixture was centrifuged at 4000 rpm for 20 minutes (min) at 20 ^{o}C. The supernatant was carefully separated and lyophilized for 6 – 8 h.

A simple solubility test confirmed the HA-COOH formation by dissolving it in DMSO.[39, 40] No further characterization was done.

Then, the nanocarriers (NCs) were synthesized using the IME method by interfacial crosslinking with TDI.[25, 26, 41] The synthesis protocol includes the preparation of an oil phase, an aqueous phase, and an additive phase. Typically, an oil phase was prepared by dissolving 200 mg hypermer B246 in 10 g cyclohexane at 60 ^{o}C. An aliquot of 2.5 g from the solution was taken to prepare the additive phase. The aqueous phase contained 5 mg of SRB dye or 10 mg of DOX, and various quantities of HA-COOH and HPD were dissolved in DMSO (1.2 ml for NC-1 to NC-3 and 1.6 ml for NC-4, Table 1) and 300 µl of NaCl (1 M), a lipophobic salt to maintain osmatic pressure.[42, 43] The SRB dye was replaced with DOX to prepare DOX-loaded NCs using the NC-4 formulation (DOX-NC-4) . The aqueous and oil phases were mixed by stirring (1000 rpm) at room temperature on a stirring plate for 1 h. Then, the preemulsion was placed in an ice bath and sonicated at 68% amplitude for 3 min (30 seconds (s) pulse on, 20s pulse off) using a Branson 450W digital Sonifier® (3/16" tip). Meanwhile, the additive phase was prepared by adding TDI (variable amounts, Table 1) and 20 µl TEA (as a catalyst) in a 2.5 g aliquot of the oil phase. This mixture was immediately added dropwise to the emulsion and reacted at room temperature for 18 – 20 h. After the reaction, the NCs were redispersed in the water phase by dropwise addition of 5 ml of cyclohexane phase to 50 ml of SDS (0.3 wt. %) solution and continued stirring for 1 h at 1000 rpm with a cap on. Afterward, the mixture was kept in an ice bath and sonicated at 30 % amplitude for 3 min (3s pulse on, 3s pulse off) using a Branson 450W digital Sonifier® (1/2" tip). Then, the mixture was left on stirring for 24 h (1000 rpm) at room temperature with a cap off for cyclohexane evaporation. The excess SDS was removed by dialyzing the redispersed sample in 900 ml MQ water for 4-5 days while replenishing the water 3 – 4 times a day using a Spectra/Pore dialysis membrane (3.5 kDa MWCO).

The formulations with better encapsulation were stored in glass vials at 4 ^{o}C and used for further characterization until one month.

Physical characterization

Dynamic light scattering (DLS)

The average size (Z_{avg}) and size distribution, polydispersity index (PDI), and zeta potential of the NCs were determined by DLS using the Malvern Zetasizer Ultra instrument. For the cyclohexane phase 10 µl of the sample was diluted in 1 ml cyclohexane and analyzed in a 12.5 mm (10 mm light path) quartz glass cuvette (Hellma Analytics), and for the redispersed phase 200 µl of the sample was diluted in 1 ml MQ and analyzed in a 12.5 mm (10 mm light path) polystyrene cuvette (Brand 7590) at 25°C. The Z_{avg} measurements were performed at backscatter (175°) with the attenuator optimally selected by the instrument. The zeta potential was determined by diluting 200 µl of the redispersed sample in 1 ml KCl (1 mM), and then 800 µl of the sample was transferred to a folded capillary cell (DTS1070, Malvern) for the measurement. Moreover, to test the stability of NC (sample NC-4) in cell media, 200 µl of the redispersed sample (solid content (SC) – 3.4 mg/ml) was added to 1 ml of cell culture media and incubated at 37 ^{o}C. Then, the Z_{avg} and PDI of NCs at 0, 2, 4, 24, 48, and 72 h were measured. Furthermore, the stability of SRB-NCs (NC-1 to NC-4, redispersed sample) stored at 4 ^{o}C was tested after one month and/or 3 months (for the SRB-NC-4 sample) by diluting 200 µl of the sample in 1 ml MQ. The ZS XPLORER software was used for analysis and the experiments were conducted in triplicates.

Encapsulation efficiency and Solid content

The encapsulation efficiency (EE) was obtained by determining the released dye or drug amount with respect to the used amount in the sample by dialyzing using a dialysis membrane bag. Briefly, the redispersed samples were transferred to a dialysis bag (Spectra/Por® Dialysis Membrane, 3.2

kDa MWCO, 11.5 mm diameter) and dialyzed against a 900 ml sink (MQ water) for 24 h without water replenishment. Then, 2 ml of sample from the sink was collected and absorbance measured using UV-Vis spectrometry (Nanodrop 2000, Thermo Scientific, Belgium) at 565 nm (excitation wavelength for SRB) and 480 nm (excitation wavelength for DOX). The unencapsulated dye amount was determined using a calibration curve of SRB dye and DOX in MQ water (0 – 5 µg/ml concentration range, $r^2 > 0.99$) (Supporting information (SI), Figure S1a and S1b), and EE was calculated using eq. 1, in which $[\text{payload}]_{\text{total}}$ is the amount of payload added in the dispersed phase and $[\text{payload}]_{\text{free}}$ is the amount of payload in the sink water after 24 h. The solid content (SC) was determined by drying 1 ml of dialyzed redispersed sample on a heating plate at 45 ^{o}C and analytical weighing. The solid content was derived using eq. 2. The EE and SC were calculated in triplicates.

$$\text{EE}\ (\%) = \frac{[\text{dye}]_{\text{total}} - [\text{dye}]_{\text{free}}}{[\text{dye}]_{\text{total}}} \times 100 \qquad \text{(eq. 1)}$$

$$\text{SC}\ (\%) = \frac{\text{Weight of dry NCs}}{\text{Weight of wet NCs}} \times 100 \qquad \text{(eq. 2)}$$

Transmission electron microscopy (TEM)

The bright field TEM micrographs of cyclohexane and redispersed samples were obtained using a TECNAI^{TM} spirit transmission electron microscope working at an accelerating voltage of 120 kV. The samples were prepared by diluting the cyclohexane NCs to 0.25 % (5 µl in 2 ml cyclohexane) and redispersed NCs to about 1.6 % (25 µl in 1.5 ml MQ water). Then, 3 µl of diluted sample was dropcasted onto a 200 mesh, copper, formvar/carbon TEM grid (TED PELLA, inc.) and dried under ambient conditions overnight. No additional staining was applied. The images were processed using TEM imaging and analysis (TIA) software. The shell thickness was determined using ImageJ software. For each formulation, fifty NCs were chosen.

Chemical characterization

Attenuated total reflectance-Fourier transform infrared (ATR-FTIR) and Nuclear magnetic resonance (NMR) spectroscopy

The chemical composition of NCs was analyzed using PerkinElmer Frontier Attenuated total reflectance-Fourier transform infrared spectroscopy (ATR-FTIR) and Nuclear magnetic resonance (NMR) spectroscopy (JEOL 400 MHz) instruments. The cyclohexane phase NCs, 3 ml, were dried at 40°C and used for further characterization. KBr pellet-based FTIR was also utilized for the powder form of precursor compounds. For ^{1}H-NMR and ^{13}C-NMR, the dried sample was dissolved in deuterated solvents. OMNIC32 and MestReNova software were used for FTIR and NMR data analysis, respectively.

High-resolution solid-state nuclear magnetic resonance spectroscopy

The solid-state ^{13}C cross-polarization/magic angle spinning (CP/MAS) NMR measurements were conducted using methods similar to procedures described elsewhere.[41, 44] For the characterization of the NC-4 sample, solid-state ^{13}C-CP/MAS NMR spectra were obtained at ambient temperature on an Agilent VNMRS DirectDrive 400 MHz spectrometer (9.4 T wide bore magnet) fitted with a T3HX 3.2 mm probe dedicated for small sample volumes and high decoupling powers. Magic angle spinning was performed at 12 kHz. The aromatic signal of hexamethyl benzene was used to determine the Hartmann-Hahn condition ($\omega_{1H} = \gamma_H B_{1H} = \gamma_C B_{1C} = \omega_{1C}$) for CP, and to calibrate the carbon chemical shift scale (132.1 ppm). The following acquisition parameters were used: a spectral width of 50 kHz, a 90^{o} pulse length of 2.5 μs, a constant spin-lock field for CP of 80 kHz, a contact time for CP of 1 ms, an acquisition time of 20 ms, a recycle delay time of 2.5 s and 3500 accumulations. High-power proton dipolar decoupling during the acquisition time was set to 80 kHz. Varian NMR software – Java-based (VNMRJ 3.2) was used for data analysis.

Cumulative release studies

The cumulative release profile of SRB encapsulated NC samples under stimuli-sensitive (GSH and HAase) conditions was obtained using the dialysis method. The release of loaded SRB dye was monitored using a UV-Vis spectrophotometer (Nanodrop 2000). Briefly, 1 ml of the dialyzed redispersed sample (SRB-NC-4, SC – 3.4 mg/ml) was diluted with 1 ml of respective conditions and transferred to a Spectra/Pore dialysis membrane (3.5 kDa MWCO). Then, the samples were exposed to 15 ml sink conditions comprising MQ water (as a control), GSH (1, 2, 5, and 10 mM) at pH 7.4, HAase (0.2, 0.4, and 0.6 mg/ml), or 10 mM GSH + 0.6 mg/ml HAase (pH 7.4), and incubated at 37 ^{o}C with gentle stirring at 200 rpm. The HAase and GSH solutions were prepared in MQ water. At regular time intervals (5, 10, 20, 30, 40, and 50 h), an aliquot of 2 ml from the sink was collected and replenished with fresh conditions. Concomitantly, the aliquot absorbance at excitation wavelength at 565 nm for SRB was measured at various time points to determine the release of dye from the NCs. The cumulative release was calculated using eq. 3. In addition, a simple filtration technique was employed to remove the dye entrapped in the sediments after 50 h cumulative release in stimuli conditions (10 mM GSH (pH 7.4) and 10 mM GSH + HAase (pH 7.4)). In brief, 500 µl of the contents from the dialysis bag were diluted with 1.5 ml of 70 % EtOH and sonicated for 10 min. Then, the samples were transferred to a Millipore membrane centrifuge tube (30 kDa MWCO) and allowed to filter (gravity-based) for 3 days at room temperature under dark conditions. The concentration of SRB in the filtrate was determined by a UV-Vis spectrophotometer. Finally, the total amount of dye released was quantified by summation of the amounts accumulated from the filtrate and the cumulative release after 50 h. A fresh NC sample batch was prepared for each experimental set up (single stimulus: HAase or GSH, and dual-stimuli: GSH + HAase conditions) and all the experiments were performed in triplicates.

$$\text{Cumulative release } (\%) = \frac{V_e \sum_{i=1}^{i=n-1} C_i + V_0 C_n}{m_0} \times 100 \qquad \text{(eq. 3)}$$

V_e = extracted volume, C_i = concentration of prior measurements, V_0 = total volume, C_n = measured concentration, and m_0 = total dye amount.

Biological characterization

Alamar Blue assay for cell viability

The biocompatibility of SRB-NC-4 was tested in healthy human dental pulp stem cells (DPSCs) and A549 lung cancer cells (ATCC CCL-185). The DOX-NC-4 was assessed on A549 cells. Alamar Blue (AB) assay protocol was performed similarly to the method stated elsewhere.[26]

DPSCs were derived from dental pulp tissue obtained from extracted wisdom teeth of healthy donors as described before[45] and approved by the medical ethical committee of Hasselt University (approved with protocol number 13/0104U). Briefly, the DPSCs were grown in cell culture media (∝-Minimum essential Medium (∝-MEM) supplemented with 1% L-glutamine, 1 % penicillin/streptomycin, and 10 % fetal bovine serum (FBS)) in 75 cm² cell culture flask at 37°C with 5% CO_2 until 80 % confluency was reached. 2 x 10^3 DPSCs were seeded in separate wells of a 96-well clear culture plate (VWR International, USA) for 72 h until 40-50 % confluency was obtained. Then, the DPSCs were exposed to 100, 75, 50, 25 µg/ml of SRB-NC-4NCs and controls (positive: 1 wt.% SDS solution and negative: MQ water, the volume same as 100 µg/ml of NCs) for 24, 48, and 72 h at 37°C with 5% CO_2.

The A549 cells were grown in F-12K Medium (Kaighn's Modification of Ham's F-12 Medium) supplemented with 10 % fetal bovine serum (FBS) in 75 cm² cell culture flask at 37°C with 5% CO_2 until 80 % confluency was reached. 5 x 10^3 A549 cells were seeded in separate wells of a 96-well clear culture plate (Greiner Bio-One GmbH, Germany) for 24 h until 30 % confluency were obtained. Then, the cells were exposed to 100, 75, 50, 25 µg/ml of SRB-NC-4 and varying concentrations of free DOX and DOX-NC-4 (SI, Table S1), prepared in cell culture medium

containing 1 % penicillin/streptomycin, and controls (positive: 1 wt.% SDS solution and negative: MQ water, the volume same as 100 µg/ml of NCs) for 24, 48, and/or 72 h at 37°C with 5% CO_2. After exposure, the medium was removed, the cells were washed with warm PBS, and then 120 µl of a 5 % AB solution in DMEM (for DPSC cells) and DMEM/F-12 (for A549 cells), both media without phenol red, was added to cells and incubated for 30 minutes at 37°C with 5% CO_2. Afterward, the fluorescence intensity (Ex/Em: 530 nm/ 595 nm) was measured with a microplate reader (Fluostar OMEGA, BMG Labtech, France was used for DPSC cells, while a CLARIOstar spectrophotometer, Isogen Lifetech, Belgium was used for A549 cells). For SRB-NC-4, each biological repeat (N=3 for DPSCs and A549 cells) had 10 technical replicates (wells) for DPSCs and 6 technical replicates for A549 cells per condition. For DOX-NC-4, each biological repeat (N=3, A549 cells) had 4 technical replicates (wells) per condition. Cell viability was assessed by subtracting the blank background (AB without cells and NCs) from all conditions, followed by calculating the percentage relative to the mean emission values of the negative control. As per ISO 10993-5, percentage of cell viability above 80 % are contemplated as non-cytotoxic; within 80 – 60 % weak; 60 – 40 % moderate; and less than 40 % are highly cytotoxic.[46, 47]

Cellular uptake studies

The SRB-NC-4 and DOX-NC-4 formulations were used for cellular uptake studies. DPSCs were seeded at a density of 1.5×10^4 cells per well (24-well plate, VWR International, USA) on ethanol-sterilized coverslips and cultured in ∝-MEM for 72 h at 37 °C with 5% CO_2 until 30 – 40 % confluence was achieved. Then, the cells were exposed to SRB-NC-4 (100 µg/ml) for 24 h at 37°C with 5% CO_2. After exposure, the media were removed, and cells were washed three times (5-minute intervals) with warm PBS and fixed with 4 % PFA (prepared in PBS) for 15 minutes. After rinsing the samples with PBS twice, the DPSC cells were stained with CellMask Green Actin

Tracking stain, (stains F-actin filaments, highlighting the intracellular cytoskeletal structure) (1:1000, prepared in PBS) for 15 minutes at room temperature and with DAPI nucleic acid stain (1:1000, prepared in PBS) for 5 minutes. Finally, the DSPCs were rinsed with PBS thrice and mounted on a glass slide using Shandon Immu-Mount (Thermo Fischer Scientific, Canada) following the manufacturer's recommendations. Cell images were acquired using a confocal microscope (ZEISS LSM 990, Germany). The Laser Scanning Microscopy (LSM) mode was applied with Diode (405 nm, 0.4 % power), Diode (488 nm, 0.3 % power), and Diode (561 nm, 0.2 % power) lasers. The emission detection wavelengths were 450 – 570 nm for CellMask green, 400 - 595 nm for DAPI, and 560 – 700 nm for SRB dye loaded in NCs. To distinguish between NCs attached to the cell surface and internalized NCs, the XYZ acquisition mode was used with 63x magnification. The confocal images were acquired using the ZEN 3.10 (ZEN lite) software.

For A549 cells exposed to SRB-NC-4 and DOX-NC-4, images were acquired using the Operetta CLS high-content imager (Revvity, USA). Briefly, 1×10^4 A549 cells per well were seeded in black 96-well Phenoplates (Revvity, USA) and cultured in F-12K Medium for 24 h at 37 °C with 5% CO_2 until 50 % confluence was achieved. Then, the cells were exposed to SRB-NC-4 (100 µg/ml) or DOX-NC-4 (concentration equivalent to DOX amount expected in the highest concentration of NCs, based on the encapsulation efficiency, SI, Table S1) for 24 h at 37°C with 5% CO_2, thereafter, they were fixed with 4% PFA. The SRB-NC-4 exposed cells were stained with Hoechst 33342 (2 µg/ml in PBS) for nucleic acid and Wheat Germ Agglutinin (WGA)-Alexa Fluor 488 (2.5 µg/ml in PBS) for the cell membrane for 10 minutes (fixing, staining, and washing protocol is similar to DPSCs, as discussed above). The A549 cells exposed to DOX-NC-4 were used for bright field imaging without staining the cell membrane and nucleus (as excitation wavelengths of WGA-Alexa Fluor 488 and DOX are in the same range). The unstained cells were

washed with PBS three times to remove dead cells and fixed with 4 % PFA. The images were acquired using Operetta CLS high-content imager with a 40x objective (water, NA 1.1). At least 15 planes with a distance of 0.5 µm were acquired using a Z-stack. The emission detection wavelengths were 500 – 550 nm for WGA-Alexa Fluor 488, 430 - 500 nm for Hoechst, and 570 – 620 nm for SRB dye loaded in NC-4 NCs. For DOX-NC-4, the excitation and emission wavelengths were 460 – 490 nm and 570 – 620 nm, respectively. The Operetta CLS images were acquired and analyzed using the Harmony 5.2 software.

Statistical Analysis

JMP Pro 16 software was used for the statistical analysis of shell thickness measurement and cell viability results. The Shapiro-Wilk test was used to verify if the data fit a normal distribution. If the data was not fitted in a normal distribution, then nonparametric tests were performed. The Wilcoxon/Kruskal-Wallis test was used to confirm the significance of the dataset. Subsequently, the Wilcoxon method was conducted to determine the significance between each pair. Data are presented as mean ± standard error or deviation and were deemed significant at a p-value smaller than 0.05 (*), 0.001 (**), and 0.0001 (***).

RESULTS AND DISCUSSION

Biopolymers, particularly polysaccharides, are frequently subjected to chemical modifications to introduce stimulus-responsive functionalities. In contrast, this work demonstrates a one-pot synthesis approach for developing responsive and biodegradable biopolymer-based nanocarriers for delivering hydrophilic compounds without the necessity for any preliminary modification of the biopolymer. This strategy offers a more cost-effective and time-efficient alternative to conventional methods, while preserving the inherent properties of the biopolymer.

HA-COOH-HPD NCs synthesis and characterization

The GSH- and HAase-responsive NCs formulations were achieved by employing the reaction between hydroxy groups (OH) of HA-COOH/HPD and isocyanate groups (N=C=O) of TDI at the interface by using the IME technique.[29] The HA-COOH is prone to enzymatic degradation, and HPD is sensitive to glutathione due to the disulfide bond. As per our knowledge, the existing work on HPD-based NCs is very limited, and it has an intriguing property when combined with biopolymers. On the one hand, HPD is a hydrophobic compound soluble in polar solvents like DMSO, making it easier to fabricate NCs via IME for hydrophilic payloads using a DMSO/water mixture. On the other hand, Na-HA is highly soluble in MQ water, but poorly soluble in DMSO. Thus, the conversion from salt Na-HA to acid form (HA-COOH) resolved the solubility issues in the aqueous phase for the homogeneous distribution of materials in the aqueous core, making it possible to develop responsive biopolymer based NCs without further chemical modification. After synthesis in the cyclohexane phase, the NCs were transferred to water containing anionic surfactant (0.3 wt.% SDS, redispersed phase) that acts as a stabilizer.[28] The excess SDS was removed via dialysis against water for 4-5 days. The fabrication procedure is depicted in Figure 1a and the reaction mechanism in Figure 1b. In all cases, no precipitation, coagulation, or flocculation of the NCs was observed throughout the process.

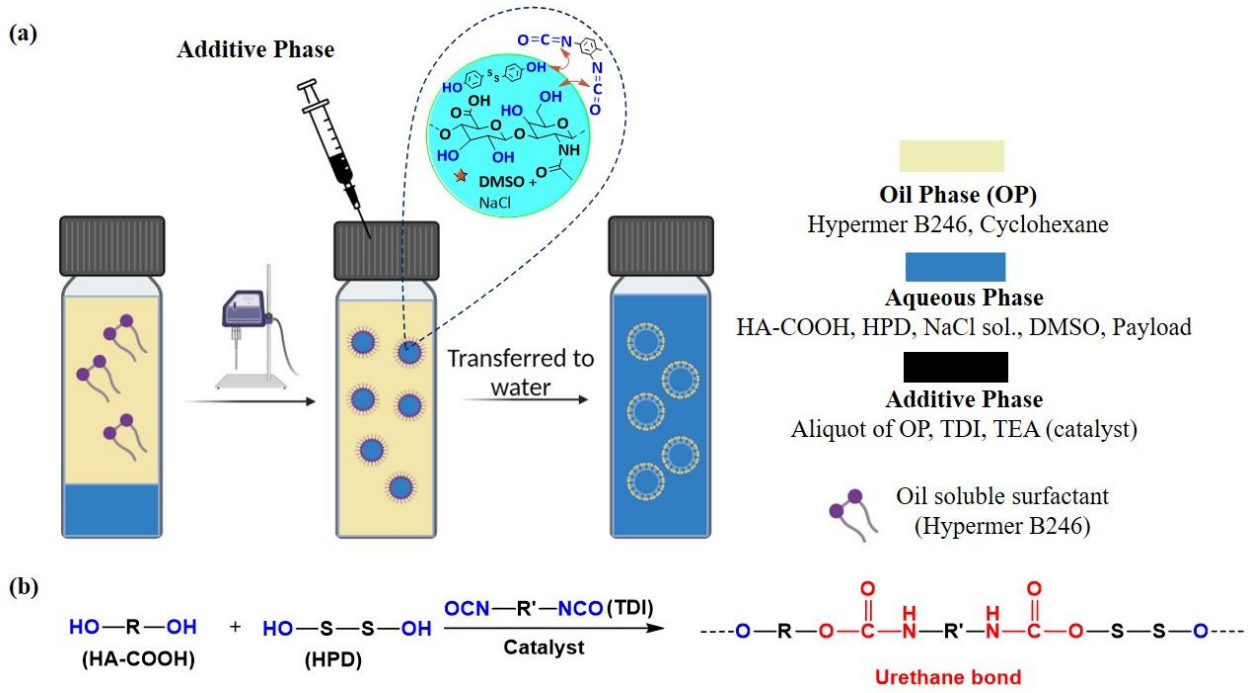

Figure 1: a) Schematic illustration of nanocarrier formation via the inverse miniemulsion method using interfacial OH-isocyanate crosslinking chemistry. After the reaction in cyclohexane phase, the NCs were transferred to water containing 0.3 wt.% of SDS, which was subsequently removed through dialysis. b) An overview of the reaction mechanism.

The SRB-dye loaded dual stimuli-responsive biopolymer-based NCs were achieved using different combinations of HPD/HA-COOH and TDI. Firstly, NCs with increasing TDI amount (150, 200, and 250 μl), while keeping HPD and HA-COOH amounts constant, were synthesized. The samples in the cyclohexane and redispersed phase was measured for their hydrodynamic size, size distribution, and surface charge (zeta potential) using DLS (Table 1). The average size (Z_{avg}) of NCs in the cyclohexane phase for samples NC-1 to NC-3 was between 140 - 153 nm with a polydispersity index (PDI) between 0.13 - 0.15, depending on the crosslinking density. The Z_{avg} of NCs in the redispersed phase was slightly larger ($\pm$ 20 nm increase), ranging from 158 to 176 for samples NC-1 to NC-3 with a PDI from 0.14 to 0.16. This could be due to the hydration layer of

SDS and hydrophilic part (polyethylene glycol) of the block copolymer hypermer B246, which is added as an emulsifying agent in the continuous phase during the synthesis.[26] These findings are in accordance with the previously reported values for polyurethane nanocapsules.[25, 41] The zeta potential values (measured in 1 mM KCl solution) of the redispersed samples both before and after dialysis were negative due to the residual presence of anionic surfactant and carboxylic groups of HA-COOH (Table 1). The decrease in the conductivity values after 4-5 days of dialysis indicates the removal of excess SDS. The EE of redispersed samples enhanced with increasing TDI amount. Up to 97 % of EE was achieved for the NC-3 formulation. Samples with TDI below 150 μl yielded lower EE (data not shown). Subsequently, the stability of the SRB dye-loaded NC-3 (SRB-NC-3) sample (SI, Figure S2) against inherent leakage was studied by monitoring the release in water at 37 ^{o}C (condition chosen as control also for release studies, cf. *vide infra*). The result demonstrated that the dye release was increased over time, indicating that the NCs are leaky. This could be attributed to the insufficient shell thickness and/ or a permeable polymeric shell. Therefore, formulation SRB-NC-4, consisting of twice the amount of HPD and HA-COOH, while keeping the TDI amount constant, was prepared. The Z_{avg} of the NC-4 sample in the cyclohexane and redispersed phase was 132 nm and 158 nm (with $\pm$ 20 nm size increase in redispersed phase), respectively, with a PDI of 0.12 and 0.14, respectively. The EE remained unchanged at 97 %, indicating that the crosslinker (TDI) amount was sufficient, even with double the amounts of HPD and HA-COOH. Additionally, the zeta potential value decreased after dialysis (Table 1). Subsequently, further characterizations were performed using the SRB-NC-4 sample formulation, and an anti-cancer drug (DOX) was encapsulated to test the potential of these NCs for biomedical applications. The DLS and EE data are shown in SI, Table S2. The Z_{avg} in cyclohexane and redispersed phase was about 156 and 197 nm, respectively. The increase in size in the cyclohexane

and redispersed phase can be attributed to the increased amount of payload when compared to SRB-NC-4 NCs. Up to 94 % of EE was achieved, indicating the ability of these NCs to hold and deliver payloads for therapeutic purposes.

Table 1: DLS results of SRB-loaded NCs in cyclohexane and water phase[a] (after dialysis).

Sample Code	Composition			CH Phase		RD phase				
	HA-COOH (mg)	HPD (mg)	TDI (μL)	Z_{avg} (nm)	PDI	Z_{avg} (nm)	PDI	ζ(mV)/ σ (mS/cm) PD	ζ(mV)/ σ (mS/cm) AD	EE (%)
NC-1	10	5	150	142± 12	0.14± 0.01	158± 3	0.14± 0.02	-30.1±5/ 0.29±0.02	-27.6±0.09/ 0.11±0.01	86±0.4
NC-2	10	5	200	140± 21	0.13± 0.02	159± 11	0.16± 0.02	-37.3±6/ 0.28±0.01	-32.1±1/ 0.12±0.01	93±0.5
NC-3	10	5	250	153± 16	0.15± 0.01	176± 11	0.16± 0.01	-43.6±3/ 0.26±0.01	-37.9±0.7/ 0.11±0.01	97±1
NC-4	20	10	250	132± 4	0.12± 0.01	158± 2	0.14± 0.01	-38.2±1/ 0.27±0.01	-30.3±2/ 0.11±0.01	97±1

[a]Zeta potential was measured before and after dialysis. The EE was determined via the dialysis method. CH, Cyclohexane; RD, Redispersed; Z_{avg}, Average particle size; PDI, Polydispersity index; ζ, Zeta potential; σ, Conductivity; PD, Prior dialysis; AD, After dialysis; EE, Encapsulation efficiency. The values are represented as mean ± standard deviation (N=3).

The stability of NC-4 in the DPSCs and A549 cells medium (with 10% FBS) at 37 ^{o}C measured using DLS (SI, Figure S3a and S3b) showed that immediately after transfer of NCs to cell media (time 0 h), a small increase in the average diameter 170 ± 3 nm with 0.17 PDI of NCs was observed in comparison to MQ water (160 ± 3 nm with 0.15 PDI), but no drastic changes were seen until 72 h. The observed size shift and broad distribution is probably due to protein adsorption onto the NCs' surface, which occurs instantly (soft biocorona) and evolves over time to a hard biocorona.[48, 49] The colloidal stability of SRB-loaded NCs in redispersed phase (stored at 4 ^{o}C) was tested for

the samples (NC-1 to NC-4) after one month (SI, Figure S4a and S4b). The average diameter and PDI remained consistent after one month for all formulations, and all the physicochemical and biological characterizations were conducted within 4 weeks after sample preparation. Moreover, the colloidal stability of the SRB-NC-4 sample (stored at 4 ^{o}C) also remained stable even after 3 months (SI, Figure S4c and S4d).

Morphology of HA-COOH-HPD NCs

The morphology of the obtained SRB-loaded NCs was studied using TEM (Figure 2). The micrographs in both cyclohexane and redispersed phase (after dialysis) demonstrated a core-shell nanocapsule morphology in all cases.[26, 41, 50] However, an increase in shell thickness was observed with higher amount of TDI (SI, Figure S5), improving the EE. Similar results were obtained in another study, where an increased amount of crosslinker was used.[51] The shell thickness enhanced from approximately 19 to 27 nm for samples NC-1 to NC-3 ($p < 0.0001$), respectively. A higher shell thickness of ~ 36 nm was noticed for sample NC-4 ($p < 0.0001$), which could be explained by increased reaction between the OH and isocyanate groups when larger amounts of HPD and HA-COOH were used. The average capsule size is slightly smaller than that measured using DLS due to the drying effect.[25] Moreover, pure HA-COOH-based NCs were synthesized with the same amount of biopolymer and TDI used in NC-4, and the morphology was compared with HPD containing NCs (NC-4). TEM micrographs showed that the NC-4 NCs have a thicker electron-dense shell in comparison to pure HA-COOH NCs (SI, Figure S6), which could be attributed to the aromatic structures in the HPD. Furthermore, the micrographs of DOX-NC-4 (SI, Figure S7) demonstrated a core-shell nanocapsule morphology in both the cyclohexane and redispersed phase, similar to the dye-loaded SRB-NC-4 sample.

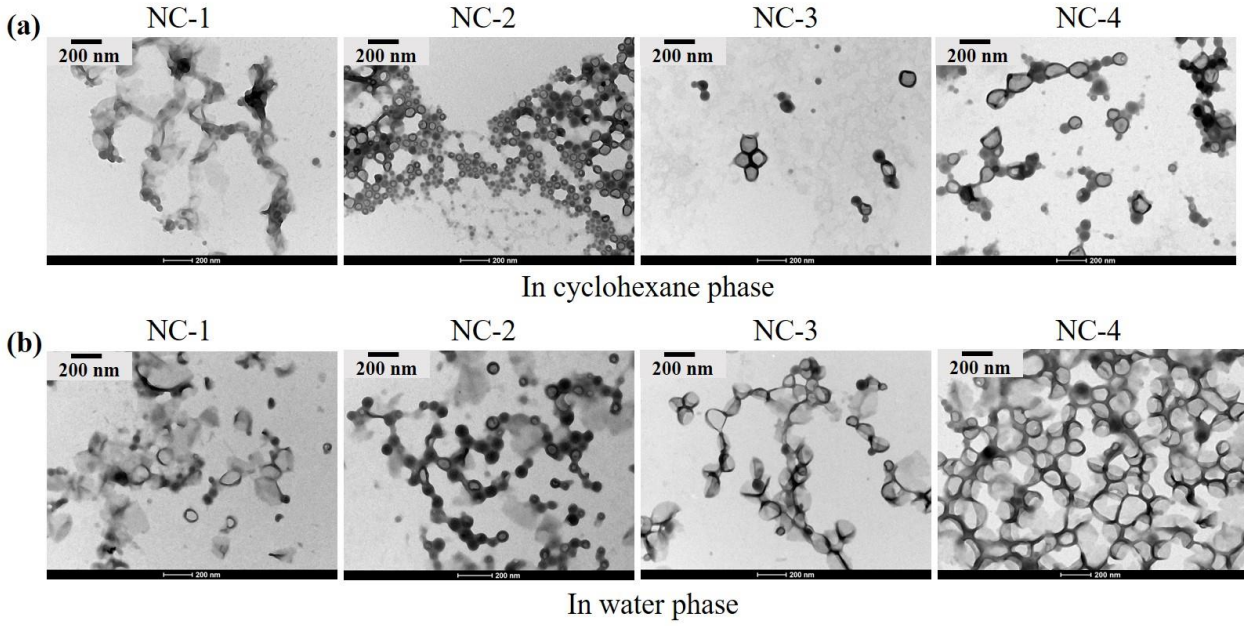

Figure 2: Transmission electron micrographs of SRB-loaded NC-1 to NC-4 in a) cyclohexane phase and b) water phase after dialysis.

Chemical analysis

The chemical composition of the dried NCs (at 40 ^{o}C) in the cyclohexane phase was first studied by ATR-FTIR spectroscopy. The spectrum of SRB-NC-4 is shown in Figure 3. The overview spectra, including all precursor compounds and SRB-NC-4, are shown in SI, Figure S8. The success of the reaction between OH and isocyanate groups is determined by urethane bond formation. A characteristic peak of the isocyanate group (2280 - 2270 cm^{-1}) has disappeared after the NCs synthesis. However, the peak at 3446 cm^{-1} can be attributed to the remaining OH groups of HA-COOH biopolymer. The presence of the N-H bending band at 1603 cm^{-1} and a carbonyl group (C=O) stretching band at 1733 cm^{-1} confirms the urethane bond formation. Similar bands were observed in the earlier reports.[28, 29, 41] Moreover, the appearance of a peak at 1695 cm^{-1} can be assigned to the urea carbonyl (C=O) group as a result of the reaction between isocyanate and amine (formed from side reactions between water and isocyanate in the aqueous phase), as reported

previously.[52] Furthermore, the residual TDI (if any remained in the cyclohexane phase) can also react with H_2O (when NCs are transferred from the cyclohexane phase to the redispersed phase). This ensures the complete consumption of isocyanate groups, assuring the safe usage of these NCs for biomedical applications.

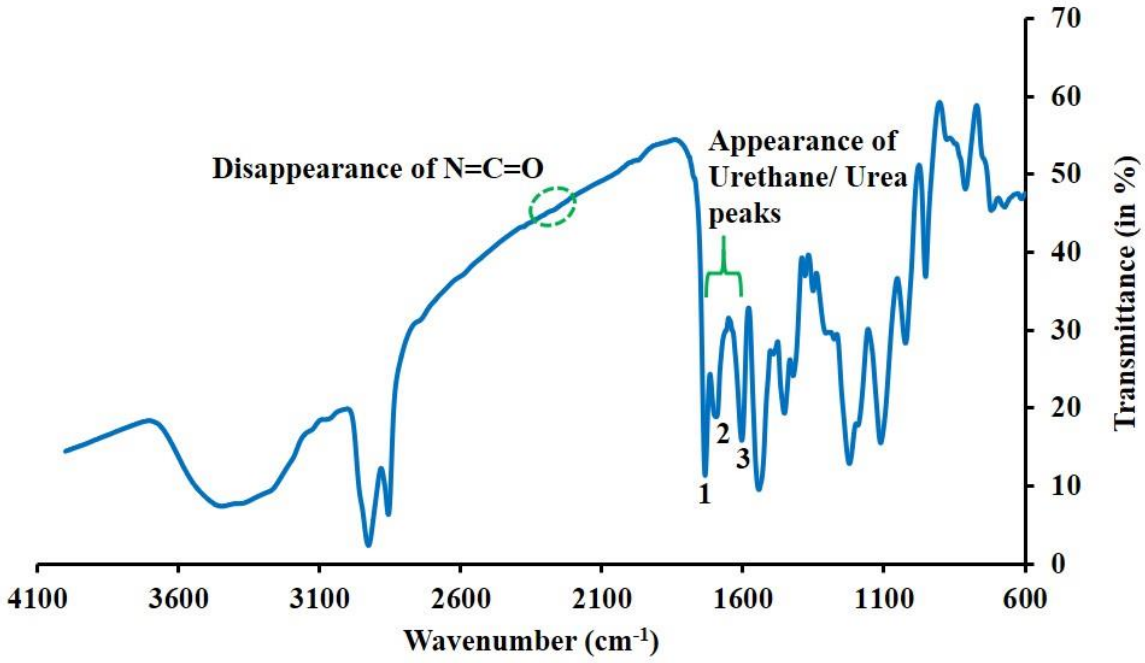

Figure 3: ATR-FTIR (KBr pellet) spectrum of SRB-NC-4 indicating the presence of urethane (peak 1 and 3, C=O, 1733 cm^{-1} and N-H, 1603 cm^{-1}) and urea (peak 2, C=O, 1695 cm^{-1}) bonds after synthesis in cyclohexane phase (after drying).

In addition to ATR-FTIR, ^{13}C liquid-state NMR data proved the formation of the urethane bond and the presence of both HPD and HA-COOH. The spectra of SRB-NC-4 and all precursor materials are shown in Figure 4. In the spectrum of HPD in Figure 4d, the peaks at 116 and 133 ppm are attributed to the protonated aromatic carbons, and the peaks at 125 and 158 ppm can be ascribed to aromatic carbons adjacent to sulfur and hydroxy groups, respectively. The glucose rings of HA-COOH are labeled in a conventional scheme, $C_{1'}$-$C_{5'}$ for glucuronic acid and C_1-C_5 for N-

acetyl-glucosamine monomeric units in the spectrum, Figure 4e. The methyl group carbon from the N-acetyl-glucosamine unit of HA-COOH is assigned at 22 ppm, the peaks at 54, 60, and 68 ppm can be attributed to C2, C6, and C4 carbons, respectively, and the peaks at 72, 73, and 75 ppm can be ascribed to C2', C3', and C5'carbons of glucuronic acid ring of HA-COOH. The anomeric carbons C1 and C1' are assigned at 101 and 102 ppm, respectively. The peaks at 171 and 174 ppm can be attributed to carbonyl carbons C6' and C7 of glucuronic and N-acetyl-glucosamine units, respectively. In the spectrum of NC-4, in Figure 4f, the peaks at 14, 17, and 22 ppm are assigned to methyl group carbons arising from Hypermer B246, TDI, and HA-COOH, respectively. The signals of the residual aliphatic carbons of Hypermer B246 are situated in the 25 – 34 ppm region. The peaks at 54, 63, and 68 ppm can be ascribed to carbons (C_2, C_6, and C_4, respectively) from the N-acetyl-glucosamine monomeric unit of HA-COOH. The peak at 70 ppm can be attributed to the ether functionalities of the surfactant (Hypermer B246, a block copolymer consisting of polyhydroxy stearic acid and polyethylene glycol moieties).[53] The anomeric carbons C1 and C1' of HA-COOH are assigned at 104 and 106 ppm, respectively. The peaks at 116 and 133 ppm are attributed to the protonated aromatic carbons of HPD, and the peaks at 125 and 158 ppm can be ascribed to aromatic carbons adjacent to sulfur and hydroxy groups of HPD, respectively. The peaks at 120 and 130 ppm can be assigned to protonated aromatic carbons of TDI, while the peak at 138 ppm can be designated as a tertiary aromatic carbon (from TDI) adjacent to the urethane bond.[54] The well-defined intense peaks at 153 and 154 ppm correspond to urea and urethane carbonyl groups, respectively, indicating the successful reaction between OH and isocyanate groups.[41] The peaks at 171 and 172 ppm can be attributed to carbonyl carbons C6' and C7 of glucuronic and N-acetyl-glucosamine units of HA-COOH, respectively. However, due to the limited solubility of the emulsion in DMSO-d6 and the low amount of biopolymer in comparison

to hypermer B246, only a few peaks of HA-COOH were observed. It is worth mentioning that small changes in the chemical shift are noticed for some peaks due to the NMR measurements in different solvents (D_2O for HA-COOH and DMSO-d6 for SRB-NC-4). For example, the chemical shift of the anomeric carbons of HA-COOH between 104 -106 ppm in the SRB-NC-4 spectrum (Figure 4f) was slightly different from their position in the spectrum of pure HA-COOH between 101 – 102 ppm (Figure 4e). Since not all HA-COOH peaks were observed in the solution spectrum in DMSO-d6, high-resolution solid-state ^{13}C-NMR was performed to observe the missing peaks of HA-COOH. The ^{13}C CP/MAS spectrum of a sample identical to NC-4 but prepared without the dye to avoid complexity in analysis is shown in Figure 5. The peaks between 18 – 40 ppm can be assigned to the methyl and aliphatic carbons from hypermer B246/ TDI/ HA-COOH. The peaks at 54 and 64 ppm can be attributed to C_2 and $C_{6,}$ respectively, and the peaks in the region 72-85 ppm to C3, C4, C5, C2', C3', C4', and C5' of the HA-COOH monomeric unit.[55] The broad distribution of peaks between 100 – 150 ppm can be designated to aromatic carbons of TDI and HPD, and anomeric carbons of HA-COOH. The broad intense peak at 154 ppm is accredited to urethane and urea carbonyl carbon (C=O), while the peak at 174 ppm can be ascribed to the carbonyl carbons ($C_{6'}$ and C_7) of HA-COOH. Similar peaks were found in the study of Grosu *et al.* in which the ^{13}C solid-state NMR of pure HA-COOH is shown.[56]

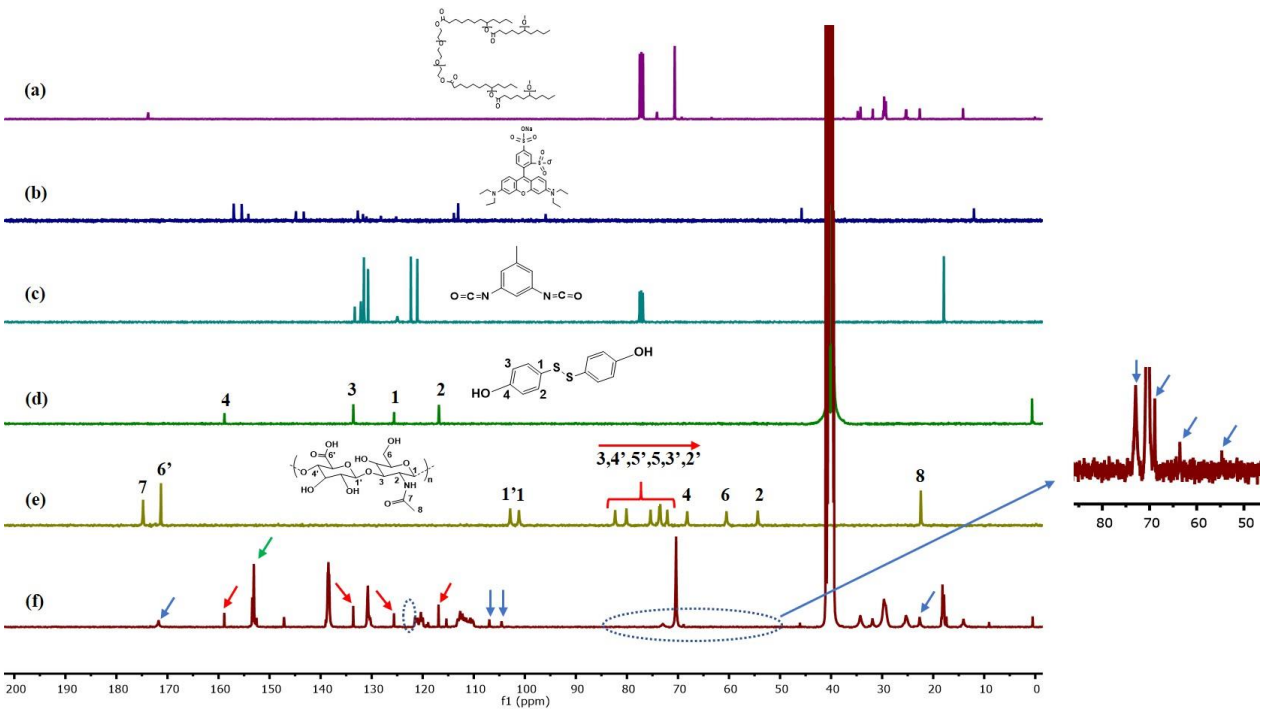

Figure 4: ^{13}C NMR (400 MHz) of precursor compounds (a-e) and SRB-NC-4 (after drying) (f). a) Hypermer B246 in $CDCl_3$; b) SRB dye in D_2O; c) TDI in $CDCl_3$; d) HPD in DMSO-d6; e) HA-COOH in D_2O (Red arrow indicates the direction from left to right); f) SRB-NC-4 in DMSO-d6 (Blue ticks indicate HA-COOH peaks, Red ticks indicate HPD peaks, Green ticks indicate urethane and urea peaks, The blue dotted circle around 120-125 ppm indicates the absence of isocyanate (N=**C**=O) carbon peaks).

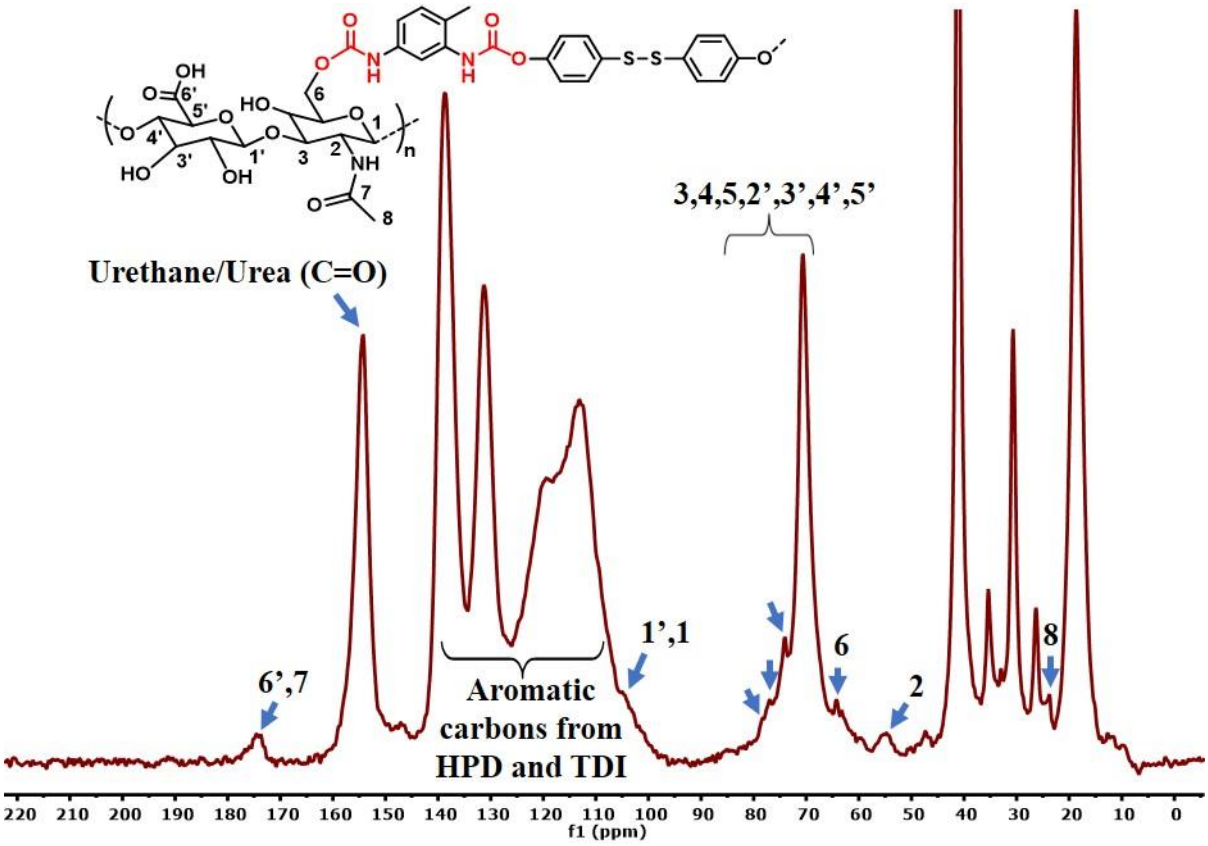

Figure 5: ^{13}C-CP/MAS solid-state NMR spectrum of NC-4 (without dye, after drying). The blue arrows indicate the biopolymer and urethane peaks.

Release studies

The cumulative release of SRB dye from NC-4 formulation was studied. Since the NCs shell contains enzyme (HAase)-sensitive HA-COOH and GSH-responsive HPD moieties, the time-dependent release of hydrophilic SRB dye was investigated in the presence of both triggers, individually and in combination. Firstly, the release was performed in different concentrations of HAase (0.2, 0.4, and 0.6 mg/ml) or GSH (1, 2, 5, and 10 mM) at physiological temperature (37 ^{o}C) and the absorbance measured at regular time intervals of 5, 10, 20, 30, 40, and 50 h. In order to demonstrate the proof of concept, a known amount of HAase was chosen based on earlier reports to study the release via enzymatic degradation.[57, 58] The latter was performed by using a

concentration range of enzyme, starting from a minimum concentration where the NCs start degrading, to a concentration where complete collapse (visually seen, Figure 6c) of the NCs due to the enzymatic degradation was observed. The sink conditions consisting of MQ water at 25 ^{o}C and 37 ^{o}C were considered controls. It was found that the SRB dye release increased when the HAase concentration was higher (Figure 6a). The percentage of release reached up to 40 % for 0.6 mg/ml of HAase after 50 h, while the control at 37 ^{o}C reached only about 10% after 20 h and approximately 20% after 50 h, while no change was observed at 25 ^{o}C after 20 h. A similar release profile was observed with increasing GSH concentrations (Figure 6b). A higher release percentage of up to 50 % was noticed for 10 mM GSH after 50 h, whereas 25 % and 21 % were observed for 5 and 2 mM GSH, respectively. No difference in the release was observed between MQ water at 37 ^{o}C (16 %) and 1 mM GSH (18 %), indicating little to no effect of GSH on NCs integrity at concentrations of 2 mM or lower. These characteristics are very intriguing for targeting the non-regenerative[59, 60] or fibrotic tissue sites and cancer types such as breast, colorectal, lung, and melanoma (where GSH concentrations are 1 – 15 mM), while preserving NCs stability in the healthy cells and extracellular pathological environments (where GSH levels are in the 2 - 20 μM range).[61] The release under control condition (MQ water) at physiological temperature could be attributed to the trapped dyes in the shell, which, upon swelling of the HA-COOH biopolymer over time, could have led to the release of the dye.[62] However, the inherent leakage was lower (Fig. 6a and 6b) compared to the NC-3 sample (SI, Figure S2). This could be attributed to the increased polymeric shell thickness from using higher amounts of monomer and polymer to form the crosslinked shell. Also, it could be ascribed to the increased hydrophobicity from HPD in the shell, which can potentially limit water absorption and eventually reduce the swelling behavior.[62] Regardless, a sustained and controlled release was observed under stimulus conditions. These results indicate that the shell

composition and thickness play a crucial role in determining the properties, such as swelling behavior and release kinetics of biopolymer-based NCs. Moreover, the degradation of NCs was also visible to the naked eye (Figure 6c and 6d), and sedimentation of NCs was noticed after only 5 - 10 h of exposure to 0.6 mg/ml HAase and 10 mM GSH. This also explains the maximum dye release reaching only up to 40 - 50 % due to the dye entrapment in the polymer matrix during sedimentation. In the latter release studies with dual- stimuli responsive conditions, a filtration technique was employed to remove the entrapped dye. After 50 h cumulative release, the content of the dialysis bag was measured for size analysis using DLS (SI, Figure S9 and S10). Interestingly, at higher HAase (0.6 mg/ml) and GSH (10 mM) concentrations, the average diameter of NCs increased from around 150 nm with PDI of 0.15 (for MQ water at 37 ^{o}C) to 479 nm with PDI of 0.4 and 4679 nm with PDI of 0.4, respectively, resulting in a broad distribution, indicating that loaded dye was released due to the NCs disruption under stimulus conditions.

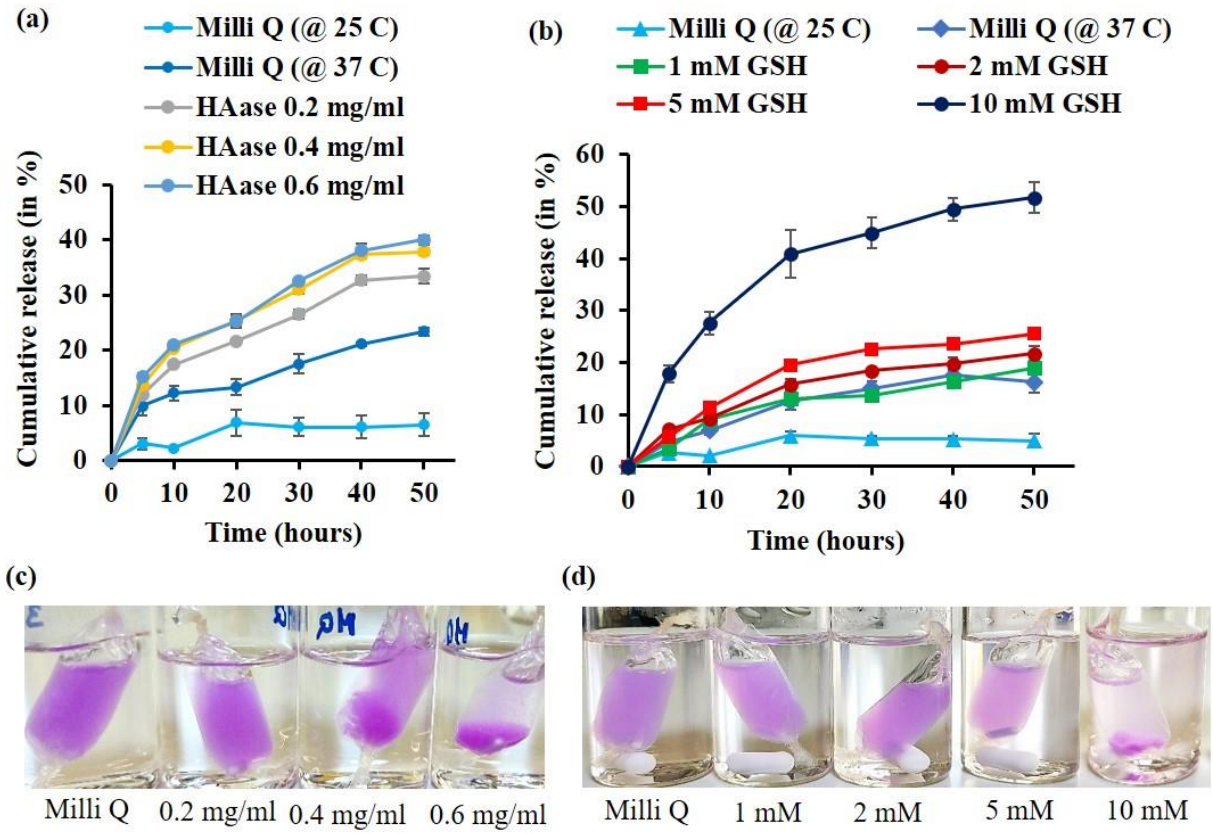

Figure 6: Cumulative release of SRB dye (λ_{ex} = 565 nm) from NC-4. a) The enzymatic-responsive release profile at different concentrations of HAase (0.2, 0.4, and 0.6 mg/ml) at 37 ^{o}C (N = 3, technical repeats). b) The GSH-responsive release profile at different concentrations (1, 2, 5, and 10 mM GSH, pH 7.4) at 37 ^{o}C (N = 3). Controls: MQ water at 25 ^{o}C and 37 ^{o}C. The error bars represent mean $\pm$ standard deviation. Visulatization of NC-4 sample after 50 h cumulative release under stimuli conditions c) HAase levels and d) GSH levels at 37 ^{o}C.

Secondly, the dual stimuli-responsive release was conducted with the highest concentrations of HAase (0.6 mg/ml) and GSH (10 mM) at pH 7.4, and compared to the dye release under a single stimulus condition (0.6 mg/ml HAase or 10 mM GSH (pH 7.4)) (Figure 7a). Again, samples in MQ water at 25 ^{o}C and 37 ^{o}C were used as controls. The results demonstrated that within the first 20 h, up to 40 % release was observed under GSH and about 35% under GSH + HAase conditions,

whereas up to 22 % release was noticed when HAase alone was used. In contrast, the release rates were significantly lower in MQ water, with only ~10 % at 25 ^{o}C and ~16 % at 37 ^{o}C after 20 h. A consistent higher release was noticed in GSH (up to 51 %) when compared to the GSH + HAase (up to 42 %) or HAase (32%) condition after 50 h. This could be explained by the fact that the GSH might inhibit the HAase activity. It has been demonstrated that the enzyme's activity deteriorated with increasing concentration of GSH due to the interaction between thiol group and hydrophobic amino acid residues of the enzyme, creating a stable complex and exerting inhibition.[63] Moreover, the degradation of NCs and sedimentation under all stimuli conditions was visually seen by naked eye after 50 h (Figure 7b). Additionally, the size of NCs measured by DLS after 50 h of cumulative release (SI, Figure S11) provided a definitive conclusion on their stability: the size of the control sample at 37 ^{o}C did not change, while the size of NCs under stimuli conditions drastically increased to the micrometer range with a PDI of 0.4. These results are further supported by the electron micrographs (Figure 8), which showed disintegration of the samples' morphology under stimuli conditions compared to the control sample. A more detrimental effect was observed under the GSH and GSH + HAase conditions. Furthermore, after the cumulative release study for 50 h, the dialysis bag contents obtained under GSH and GSH + HAase conditions were diluted with 70% EtOH, which dissolves the dye and surfactants in the polymer matrix, and transferred to the Millipore membrane tubes (Figure 9a) to remove the entrapped dye in the sediments. The results (Figure 9b) showed that overall, 90 % of the loaded dye was released in the dual-stimuli condition from both the cumulative release experiment and the filtration method. Interestingly, a higher amount of dye was observed under the combination of GSH + HAase condition when compared to GSH alone (Figure 9b). This could be interpreted from the cumulative release (Figure 7a). A slightly higher dye release at 5 h of cumulative release clearly shows the dual responsiveness, which might have

resulted in more damage to the shell in the first few hours. These collective results from different approaches unambiguously demonstrate the dual-responsive property of the NC-4 sample.

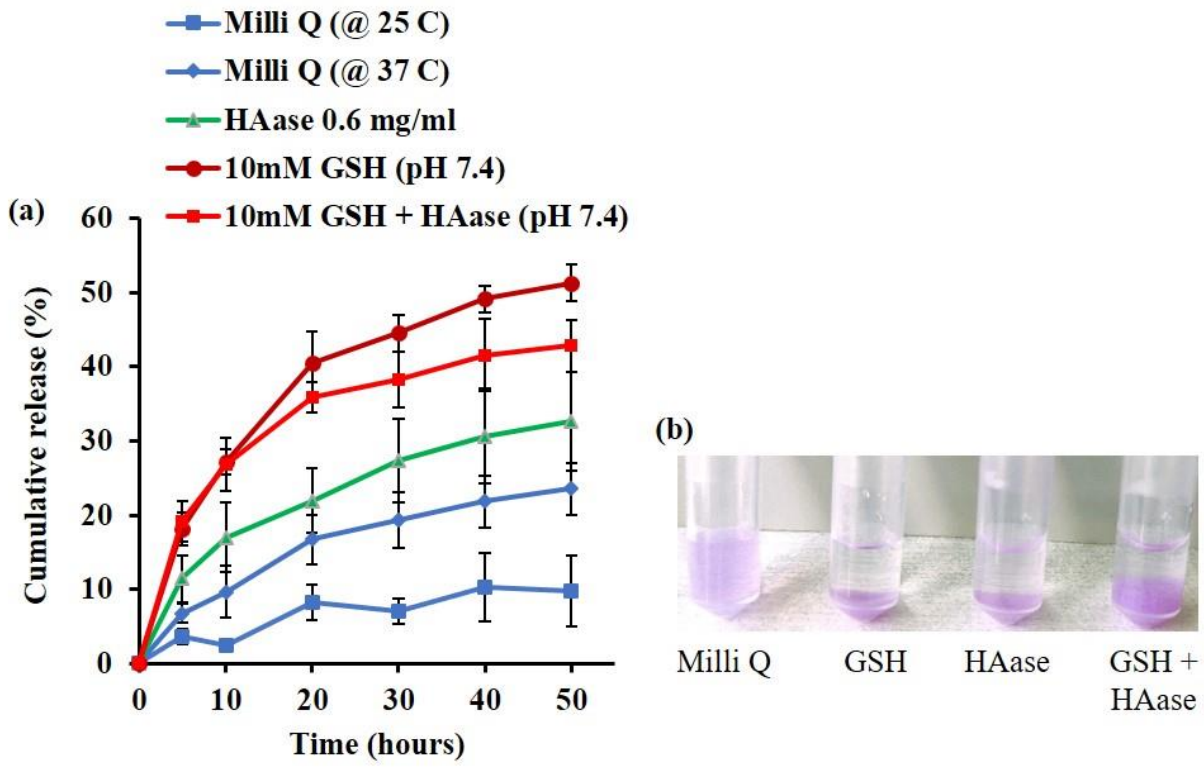

Figure 7: Cumulative release of SRB dye (λ_{ex} = 565 nm) from NC-4. a) Dual stimuli-responsive (GSH and Enzymatic) release profile of NCs under HAase 0.6 mg/ml, 10 mM GSH (pH 7.4), and 10 mM GSH + 0.6 mg/ml HAase (pH 7.4) conditions at 37 ^{o}C (error bars represent mean $\pm$ standard deviation, N=3). Controls: MQ water at 25 ^{o}C and 37 ^{o}C. b) Visualization of NC-4 sample dialysis bag content after 50 h cumulative release at stimuli conditions at 37 ^{o}C.

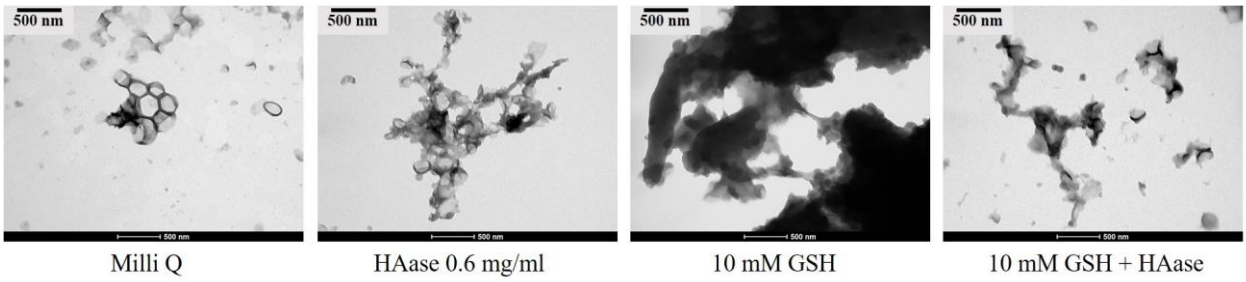

Figure 8: Representative transmission electron micrographs of SRB-NC-4 after 50 h cumulative release. Control (MQ water at 37 ºC) and after treatment with stimuli-responsive triggers: HAase 0.6 mg/ml, 10 mM GSH (pH 7.4), and 10 mM GSH + 0.6 mg/ml HAase (pH 7.4) at 37 ºC. Scale bar: 500 nm. The degree of damage: 10 mM GSH (pH 7.4) > 10 mM GSH + HAase (pH 7.4) > HAase 0.6 mg/ml > Milli Q.

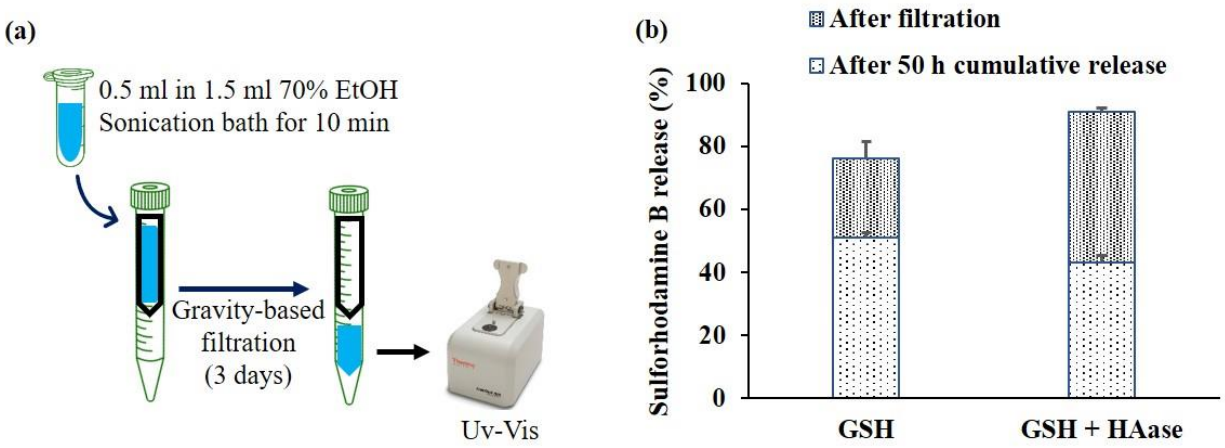

Figure 9: The amount of SRB dye accumulated from SRB-NC-4 after 50 h of cumulative release via gravity-based filtration method. a) Schematic presentation of filtration setup. Millipore Amicon Ultra Centrifugal Filter was used (30 k MWCO). b) Quantification of dye amount in 10 mM GSH (pH 7.4) and 10 mM GSH + HAase (pH 7.4) conditions using UV-Vis spectroscopy (error bars represent mean ± standard deviation, N=3).

Cell viability and uptake of HA-COOH-HPD NCs

The cell viability and uptake of SRB-NC-4 NCs were studied in healthy (DPSCs) and cancer cells (A549), while DOX-NC-4 was studied in A549 cells. The SRB-NC-4 was administered in different concentrations (25, 50, 75, and 100 μg/ml) to the DPSCs for 24, 48, and 72 h for the biocompatibility assessment (Figure 10a). The results revealed complete loss of cell viability after treatment with 1 wt. % SDS (positive control) and a slight reduction in cell viability at all concentrations of NCs (25 ($p < 0.001$), 50 ($p < 0.0001$), 75 ($p < 0.001$), and 100 μg/ml ($p < 0.001$)) after 48 h as compared to the negative control. No noticeable cytotoxic effects were observed after 72 h of exposure, suggesting favorable biocompatibility of the designed NCs. In all tested conditions, cell viability consistently remained above 80 %. These results indicate that SRB-NC-4 can be considered biocompatible as per ISO standards.[46] It is important to note that SDS, used during formulation, was removed through continuous dialysis for 4 days by replenishing the water 3 – 4 times a day, ensuring the removal of excess SDS. As a result, no potential toxicity due to residual SDS was observed across all used concentrations of the NCs.

To demonstrate the potential application of these NCs, as a proof of concept, A549 cells were exposed to DOX-NC-4 in different concentrations (SI, Table S1) for 24, 48, and 72 h for the cytotoxicity test (Figure 11a). The results revealed a dose-dependent decrease in cell viability over time. The percentage of viable cells reduced to 55 % for DOX-NC-4 after 72 h, whereas complete loss of cells was observed for free DOX at a 2 μg/ml concentration (concentration equivalent to free DOX amount expected in the highest concentration of NCs, based on the encapsulation efficiency) in comparison to the negative control ($p < 0.0001$). This difference can be attributed to the gradual diffusion of DOX from NCs, leading to a more gradual impact on cell viability. Despite that, the DOX-NC-4 still exhibited a pronounced cytotoxic effect against cancer cells, highlighting

their therapeutic usage. The biocompatibility of SRB-NC-4 NCs was also confirmed in A549 cells, and the results are shown in SI, Figure S12a.

Confocal microscopy studies displayed the uptake of the SRB-NC-4 NCs in DPSCs after 24 h of incubation (Figure 10b). Additionally, the images of A549 cells (after DOX-NC-4 and SRB-NC-4 incubation for 24 h) (Figure 11b and SI, Figure S12b) acquired using the Operetta CLS high-content imager demonstrated the intracellular uptake of NCs. The NCs were internalized and localized in clusters within the cytoplasm. The above results confirm that the NC-4 formulation is promising for drug delivery applications.

In the context of serum proteins' interaction with NCs, the studies were performed by incubating SRB-NC-4 in cell culture medium (supplemented with 10 % FBS). The observed size increase (SI, Figure S3a and S3b) indicates the formation of a protein corona around the NCs, which may alter the surface properties, impacting the release behavior.[64] Adsorbed proteins may create a barrier that hinders the diffusion of the encapsulated drugs, leading to slower release rates.[64] However, the cell viability experiments with DOX-NC-4 (Figure 11a) clearly revealed the impact on A549 cells. The dose-dependent decrease in cell viability indicates the intracellular release of DOX, implying a minimal to no influence of protein corona on the stimuli-responsive behavior. These results demonstrate the benefits of such robust yet functional NCs for therapeutic purposes.

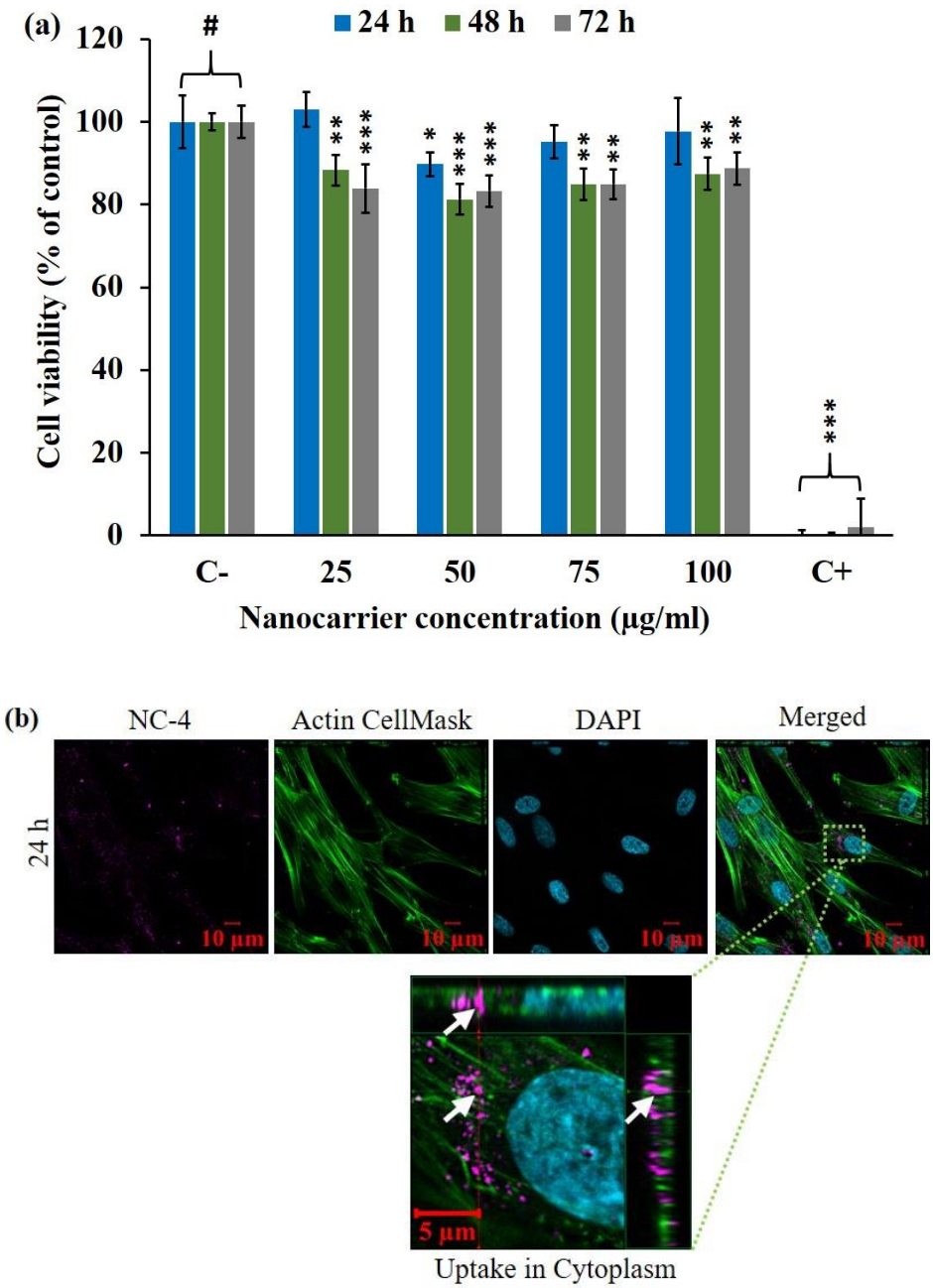

Figure 10: a) Cell viability of DPSCs determined using the Alamar Blue assay after 24, 48, and 72 h exposure to sample SRB-NC-4. Negative control (C-) = MQ water and Positive control (C+) = 1 wt.% SDS solution. Data represent mean ± standard error, N = 3. C- is used a reference for statistical testing (#). Asterisks indicate p-values < 0.05 (*), < 0.001 (**), and < 0.0001 (***).

Statistical analysis: Shapiro-Wilk method for Goodness-of-Fit test for distribution. Wilcoxon/Kruskal-Wallis Tests and Nonparametric comparisons for each pair using the Wilcoxon Method. b) Confocal micrographs of DPSCs treated with SRB-NC-4 (Violet) for 24 h. The cell membrane is stained with CellMask Green Actin Tracking stain (Green) and the nucleus with DAPI (blue). The scale bar represents 10 μm. The bottom magnified z-stack images show the uptake in the cytoplasm. The arrows indicate the NC-4 in Z-stack (XZ and YZ planes).

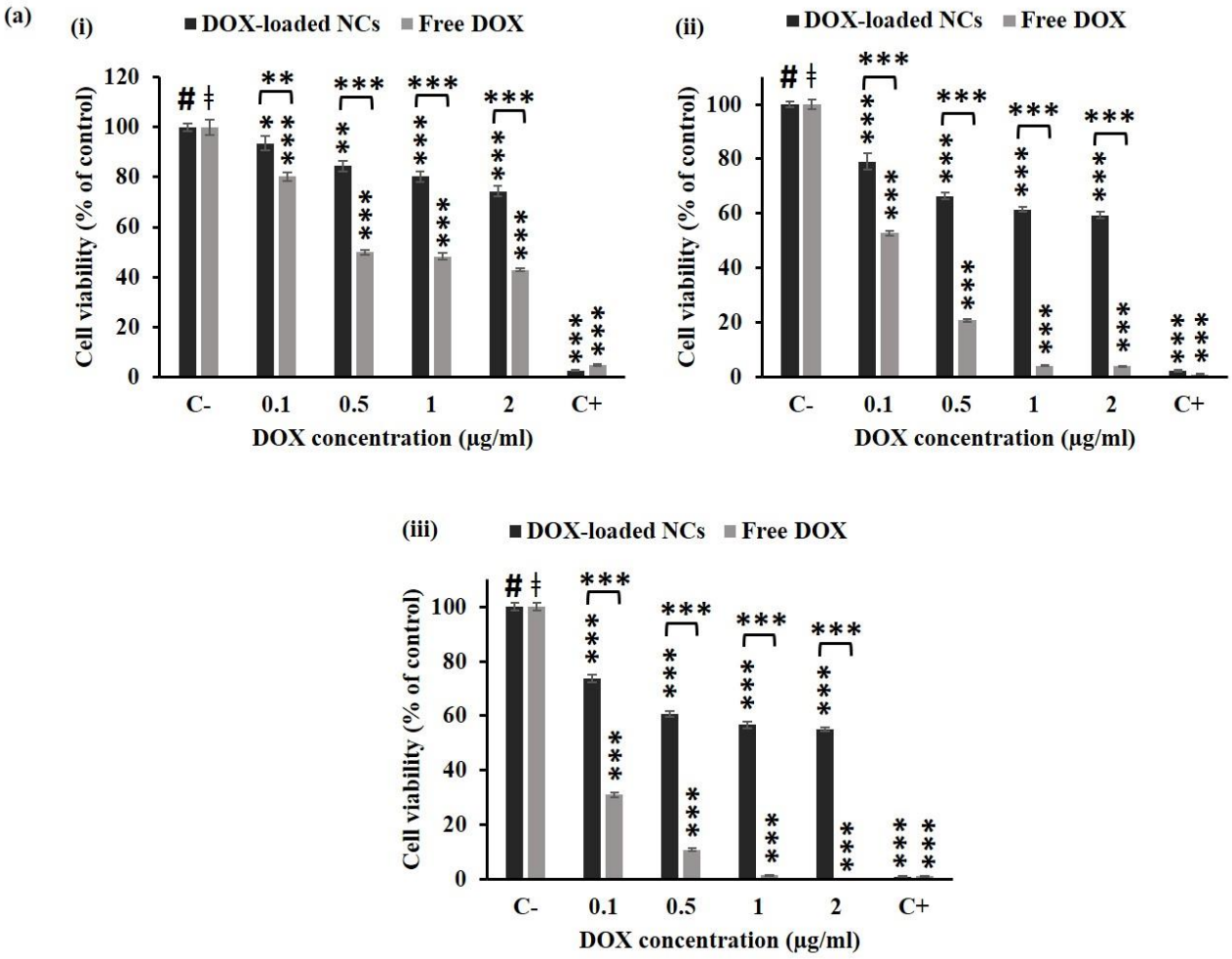

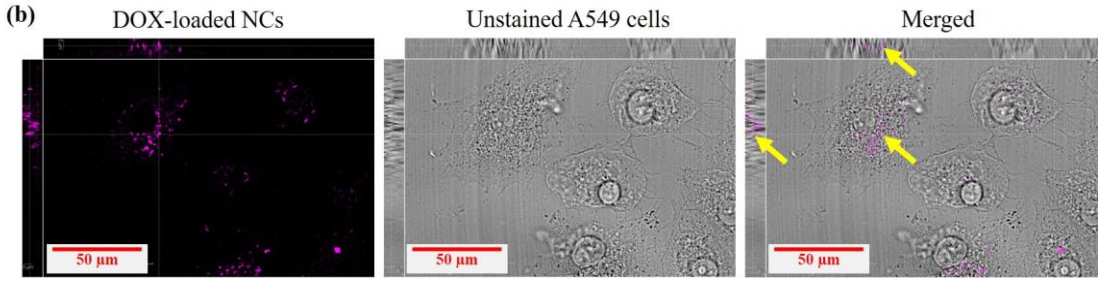

Figure 11: a) Cell viability of A549 cells determined using the Alamar Blue assay after i) 24, ii) 48, and iii) 72 h exposure to DOX-NC-4 and free DOX. Negative control (C-) = MQ water and Positive control (C+) = 1 wt.% SDS solution. Data represent mean ± standard error, N = 3. C- is used as a reference for statistical testing (# for DOX-NC-4 and ǂ for free DOX). Asterisks indicate p-values < 0.05 (*), < 0.001 (**), and < 0.0001 (***). Statistical analysis: Shapiro-Wilk method for Goodness-of-Fit test for distribution. Wilcoxon/Kruskal-Wallis Tests and Nonparametric comparisons for each pair using the Wilcoxon Method. b) Operetta CLS high-content imager bright-field micrographs of A549 cells treated with DOX-NC-4 (Violet) for 24 h. Scale bar represents 50 μm. The merged image shows the uptake in the cytoplasm. The arrows indicate the DOX-NC-4 in Z-stack (XZ and YZ planes).

CONCLUSION and OUTLOOK

Biocompatible and biodegradable dual-stimuli sensitive (GSH and HAase) HA-based nanocarriers encapsulating a hydrophilic payload were developed using the inverse miniemulsion technique employing the interfacial (OH – isocyanate) crosslinking reaction at the droplet interface. NCs with high encapsulation efficiency were successfully synthesized and displayed a core-shell nanocapsule morphology within the nanometer range (< 200 nm). The resultant urethane bond from OH and isocyanate was confirmed by ATR-FTIR and NMR spectroscopy. The cumulative release of encapsulated hydrophilic dye from NCs clearly demonstrated sensitivity toward different concentrations of single stimulus conditions of GSH and HAase, and their combination. The results

from DLS and TEM micrographs also provided evidence of the degradation of NCs under the different stimuli conditions that were tested. The Alamar blue assay for the biocompatibility test demonstrated a slight decrease in the viability of both DPSCs and A549 cells at higher concentrations of SRB-NC-4. However, cell viability remained above 80 % for DPSCs and A549 cells across all conditions. A dose-dependent cell death of A549 cells was observed for DOX-NC-4 over time. Confocal images showed the NCs uptake in both DPSCs and A549 cells.

The nanocarrier's ability to load and deliver bio-active compounds like DOX to treat lung cancer demonstrates its versatility for various therapeutic applications. These findings pave the way for useful implementations of such NCs to encapsulate and deliver other relevant hydrophilic bio-active payloads, such as proteins and nucleic acids. There is a growing interest in using them for therapeutic purposes due to their ability to target specific biological processes.[65] Despite their potential benefits, delivering them is challenging because of their low half-life, enzymatic degradation, and immunogenicity.[4] In this context, such NCs can be highly beneficial due to their hydrophilic core, which can provide a protective environment and enhance the stability of the complex therapeutic agents during storage and transport.[66]

With these promising HA-based NCs, further investigations of the endocytic pathway involved in the cellular uptake of these NCs are foreseen, as CD44 receptors are overexpressed in most cancer types and inflammatory diseases. Such studies will enhance the potential of NC-4 NCs loaded with relevant therapeutics and open new avenues in the treatment of various diseases. In addition, studies of these NCs using in-vivo tumor models overexpressing CD44 receptors may further clarify their targeting potential and biodistribution, and thus their ability for clinical translation. The CD44 targeting enhances the accumulation of these NCs more in tumor tissues, however, they may also target healthy cells as they express CD44 receptors. In here, the stimulus-sensitive property of

SRB-NC-4 NCs (Figure 6b) to remain intact in glutathione levels relevant to a healthy environment, while releasing the payload only in the presence of concentrations of glutathione relevant to the tumor environment, is highly appealing for in vivo application.

In conclusion, NC-4 NCs have potential applications in the biomedical field, including tissue regeneration and cancer therapy for delivering hydrophilic bio-active compounds without the need for chemical conjugation, thus preserving their innate biological activity. This concept can be extended to designing other responsive biopolymer-based NCs, specifically using hydrophilic polysaccharides in combination with small-molecule responsive linkers without chemical modification of the biopolymer for delivering therapeutics.

ASSOCIATED CONTENT

Supporting Information

Additional experimental results, including calibration curve of the used hydrophilic dye, cumulative release profile of NC-3 sample, DLS results of nanocarriers in cell media, shell thickness and additional TEM micrographs of all nanocarrier formulations, ATR-FTIR spectra, DLS results of nanocarriers under control and stimuli conditions, and additional cellular uptake images (DOC file).

AUTHOR INFORMATION

Corresponding Author

Anitha Ethirajan (Email – anitha.ethirajan@uhasselt.be)

Hasselt University, Institute for Materials Research (imo-imomec), Nanobiophysics and Soft Matter Interfaces (NSI) group, Martelarenlaan 42, B-3500 Hasselt, Belgium.

imec, imo-imomec, Wetenschapspark 1, B-3590 Diepenbeek, Belgium

Author Contributions

The manuscript was written through contributions of all authors. All authors have given approval to the final version of the manuscript.

ACKNOWLEDGEMENTS

The authors acknowledge the financial support from the Special Research Fund (BOF) program of Hasselt University (B20KP07, BOF21GP08). Alessia Pancaro is a Research Foundation Flanders (FWO) post-doctoral fellow (12AR624N). The FWO and Hasselt University are acknowledged for the NMR support of this research (AUHL/15/2-GOH3816N). We acknowledge the Advanced Optical Microscopy Centre at Hasselt University for support with the microscopy experiments and the microscopy was made possible by FWO project I001222N. This work is further supported by Hasselt University (IMO-IMOMEC) and VITO. Dr. S. Smeets (Applied and Analytical Chemistry, NMR facility, IMO-IMOMEC, Hasselt University) and S. Duwe (Advanced Optical Microscopy Centre, Hasselt University) are thanked for NMR and Confocal microscopy measurements, respectively. Prof. J. D'Haen (Analytical & Microscopical Services, IMO-IMOMEC, Hasselt University) and Mrs. H. Penxten (Materials Chemistry Research Group, IMO-IMOMEC, Hasselt University) are thanked for providing access to the TEM and ATR-FTIR instruments, respectively.

REFERENCES

(1) Mollazadeh, S.; Mackiewicz, M.; Yazdimamaghani, M. Recent advances in the redox-responsive drug delivery nanoplatforms: A chemical structure and physical property perspective. *Materials Science & Engineering: C* **2021**, *118*, 111536. DOI: 10.1016/j.msec.2020.111536.
(2) Meng, X.; Shen, Y.; Zhao, H.; Lu, X.; Wang, Z.; Zhao, Y. Redox-manipulating nanocarriers for anticancer drug delivery: a systematic review. *Journal of Nanobiotechnology* **2024**, *22* (1), 587. DOI: 10.1186/s12951-024-02859-w.
(3) Shi, X.; Tian, Y.; Zhai, S.; Liu, Y.; Chu, S.; Xiong, Z. The progress of research on the application of redox nanomaterials in disease therapy. *Frontiers in Chemistry* **2023**, *11*, 1115440. DOI: 10.3389/fchem.2023.1115440.
(4) Hawthorne, D.; Pannala, A.; Sandeman, S.; Lloyd, A. Sustained and targeted delivery of hydrophilic drug compounds: A review of existing and novel technologies from bench to bedside. *Journal of Drug Delivery Science and Technology* **2022**, *78*, 103936. DOI: 10.1016/j.jddst.2022.103936.

(5) Pandey, R. P.; Vidic, J.; Mukherjee, R.; Chang, C. M. Experimental Methods for the Biological Evaluation of Nanoparticle-Based Drug Delivery Risks. *Pharmaceutics* **2023**, *15* (2), 612. DOI: 10.3390/pharmaceutics15020612.
(6) Yang, C.; Wang, X.; Yao, X.; Zhang, Y.; Wu, W.; Jiang, X. Hyaluronic acid nanogels with enzyme-sensitive cross-linking group for drug delivery. *Journal of Controlled Release* **2015**, *205*, 206-217. DOI: 10.1016/j.jconrel.2015.02.008.
(7) Alipoor, R.; Ayan, M.; Hamblin, M. R.; Ranjbar, R.; Rashki, S. Hyaluronic Acid-Based Nanomaterials as a New Approach to the Treatment and Prevention of Bacterial Infections. *Frontiers in Bioengineering and Biotechnology* **2022**, *10*, 913912. DOI: 10.3389/fbioe.2022.913912.
(8) Chandra, J.; Molugulu, N.; Annadurai, S.; Wahab, S.; Karwasra, R.; Singh, S.; Shukla, R.; Kesharwani, P. Hyaluronic acid-functionalized lipoplexes and polyplexes as emerging nanocarriers for receptor-targeted cancer therapy. *Environmental Research* **2023**, *233*, 116506. DOI: 10.1016/j.envres.2023.116506.
(9) Salathia, S.; Gigliobianco, M. R.; Casadidio, C.; Di Martino, P.; Censi, R. Hyaluronic Acid-Based Nanosystems for CD44 Mediated Anti-Inflammatory and Antinociceptive Activity. *International Journal of Molecular Sciences* **2023**, *24* (8), 7286. DOI: 10.3390/ijms24087286.
(10) Pedrosa, S. S.; Pereira, P.; Correia, A.; Gama, F. M. Targetability of hyaluronic acid nanogel to cancer cells: In vitro and in vivo studies. *European Journal of Pharmaceutical Sciences* **2017**, *104*, 102-113. DOI: 10.1016/j.ejps.2017.03.045.
(11) Cheng, X.; Li, H.; Ge, X.; Chen, L.; Liu, Y.; Mao, W.; Zhao, B.; Yuan, W. E. Tumor-Microenvironment- Responsive Size-Shrinkable Drug-Delivery Nanosystems for Deepened Penetration Into Tumors. *Frontiers in Molecular Biosciences* **2020**, *7*, 576420. DOI: 10.3389/fmolb.2020.576420.
(12) Fu, C. P.; Cai, X. Y.; Chen, S. L.; Yu, H. W.; Fang, Y.; Feng, X. C.; Zhang, L. M.; Li, C. Y. Hyaluronic Acid-Based Nanocarriers for Anticancer Drug Delivery. *Polymers* **2023**, *15* (10), 2317. DOI: 10.3390/polym15102317.
(13) Mohammed, M.; Devnarain, N.; Elhassan, E.; Govender, T. Exploring the applications of hyaluronic acid-based nanoparticles for diagnosis and treatment of bacterial infections. *Wiley Interdisciplinary Reviews Nanomedicine and Nanobiotechnology* **2022**, *14* (4), e1799. DOI: 10.1002/wnan.1799.
(14) Fabozzi, A.; Della Sala, F.; di Gennaro, M.; Borzacchiello, A. Synthesis of hyaluronic acid core–shell nanoparticles via simple microfluidic-assisted nanoprecipitation method for active tumor targeting. *New Journal of Chemistry* **2022**, *46* (41), 19763-19772. DOI: 10.1039/d2nj03279a.
(15) Long, Y.-H.; Ju, X.-J.; Yang, S.-H.; Chen, S.-K.; Xie, R.; Wang, W.; Liu, Z.; Pan, D.-W.; Chu, L.-Y. Microfluidic Fabrication of Monodisperse Hyaluronic Acid Microspheres with Excellent Biocompatibility and Tunable Physicochemical Properties. *Industrial & Engineering Chemistry Research* **2024**, *63* (15), 6632-6643. DOI: 10.1021/acs.iecr.4c00337.
(16) Kwon, M. Y.; Wang, C.; Galarraga, J. H.; Pure, E.; Han, L.; Burdick, J. A. Influence of hyaluronic acid modification on CD44 binding towards the design of hydrogel biomaterials. *Biomaterials* **2019**, *222*, 119451. DOI: 10.1016/j.biomaterials.2019.119451.
(17) Chiesa, E.; Greco, A.; Riva, F.; Dorati, R.; Conti, B.; Modena, T.; Genta, I. Hyaluronic Acid-Based Nanoparticles for Protein Delivery: Systematic Examination of Microfluidic Production Conditions. *Pharmaceutics* **2021**, *13* (10), 1565. DOI: 10.3390/pharmaceutics13101565.

(18) Oommen, O. P.; Garousi, J.; Sloff, M.; Varghese, O. P. Tailored doxorubicin-hyaluronan conjugate as a potent anticancer glyco-drug: an alternative to prodrug approach. *Macromolecular Bioscience* **2014**, *14* (3), 327-333. DOI: 10.1002/mabi.201300383.
(19) Shariatinia, Z. Big family of nano- and microscale drug delivery systems ranging from inorganic materials to polymeric and stimuli-responsive carriers as well as drug-conjugates. *Journal of Drug Delivery Science and Technology* **2021**, *66*, 102790. DOI: 10.1016/j.jddst.2021.102790.
(20) Hou, J.; Zhao, Y.; Sun, L.; Zou, X. Enzyme/GSH/pH-responsive hyaluronic acid grafted porous silica nanocarriers bearing Ag(2)S QDs for fluorescence imaging and combined therapy. *Carbohydrate Polymers* **2023**, *305*, 120547. DOI: 10.1016/j.carbpol.2023.120547.
(21) Jin, R.; Liu, Z.; Bai, Y.; Zhou, Y.; Chen, X. Multiple-Responsive Mesoporous Silica Nanoparticles for Highly Accurate Drugs Delivery to Tumor Cells. *ACS Omega* **2018**, *3* (4), 4306-4315. DOI: 10.1021/acsomega.8b00427.
(22) Landfester, K. Miniemulsion polymerization and the structure of polymer and hybrid nanoparticles. *Angewandte Chemie International Edition* **2009**, *48* (25), 4488-4507. DOI: 10.1002/anie.200900723.
(23) Peters, M.; Desta, D.; Seneca, S.; Reekmans, G.; Adriaensens, P.; Noben, J. P.; Hellings, N.; Junkers, T.; Ethirajan, A. PEGylating poly(p-phenylene vinylene)-based bioimaging nanoprobes. *Journal of Colloid and Interface Science* **2021**, *581* (Part B), 566-575. DOI: 10.1016/j.jcis.2020.07.145.
(24) Peters, M.; Seneca, S.; Hellings, N.; Junkers, T.; Ethirajan, A. Size-dependent properties of functional PPV-based conjugated polymer nanoparticles for bioimaging. *Colloids and Surfaces B: Biointerfaces* **2018**, *169*, 494-501. DOI: 10.1016/j.colsurfb.2018.05.055.
(25) Seneca, S.; Pramanik, S. K.; D'Olieslaeger, L.; Reekmans, G.; Vanderzande, D.; Adriaensens, P.; Ethirajan, A. Nanocapsules with stimuli-responsive moieties for controlled release employing light and enzymatic triggers. *Materials Chemistry Frontiers* **2020**, *4* (7), 2103-2112. DOI: 10.1039/d0qm00244e.
(26) Kuypers, S.; Pramanik, S. K.; D'Olieslaeger, L.; Reekmans, G.; Peters, M.; D'Haen, J.; Vanderzande, D.; Junkers, T.; Adriaensens, P.; Ethirajan, A. Interfacial thiol-isocyanate reactions for functional nanocarriers: a facile route towards tunable morphologies and hydrophilic payload encapsulation. *Chemical Communications* **2015**, *51* (87), 15858-15861. DOI: 10.1039/c5cc05258k.
(27) Elzayat, A.; Adam-Cervera, I.; Alvarez-Bermudez, O.; Munoz-Espi, R. Nanoemulsions for synthesis of biomedical nanocarriers. *Colloids and Surfaces B: Biointerfaces* **2021**, *203*, 111764. DOI: 10.1016/j.colsurfb.2021.111764.
(28) Nayak, S.; Vanheusden, C.; Leendertse, T.; Schruers, L.; Luyck, B.; Merchiers, J.; D'Haen, J.; Buntinx, M.; Reddy, N.; Ethirajan, A. Centrifugally spun hybrid polyhydroxyalkanoate/dextran nanocapsule fiber matrix for the delivery of hydrophilic payloads. *Colloids and Surfaces A: Physicochemical and Engineering Aspects* **2023**, *675*, 132043. DOI: 10.1016/j.colsurfa.2023.132043.
(29) Nayak, S.; Caz, N.; Derveaux, E.; Smeets, S.; Cardeynaels, T.; Wolfs, E.; Adriaensens, P.; Maes, W.; Ethirajan, A. Reactive oxygen species responsive dextran-thioketal conjugate nanocarriers for the delivery of hydrophilic payloads. *Carbohydrate Polymers* **2025**, *356*, 123375. DOI: 10.1016/j.carbpol.2025.123375.

(30) Huppe, N.; Schunke, J.; Fichter, M.; Mailander, V.; Wurm, F. R.; Landfester, K. Multicomponent encapsulation into fully degradable protein nanocarriers via interfacial azide-alkyne click reaction in miniemulsion allows the co-delivery of immunotherapeutics. *Nanoscale Horizons* **2022**, *7* (8), 908-915. DOI: 10.1039/d2nh00243d.
(31) Ding, Y.; Dai, Y.; Wu, M.; Li, L. Glutathione-mediated nanomedicines for cancer diagnosis and therapy. *Chemical Engineering Journal* **2021**, *426*, 128880. DOI: 10.1016/j.cej.2021.128880.
(32) Forman, H. J.; Zhang, H.; Rinna, A. Glutathione: overview of its protective roles, measurement, and biosynthesis. *Molecular Aspects of Medicine* **2009**, *30* (1-2), 1-12. DOI: 10.1016/j.mam.2008.08.006.
(33) McAtee, C. O.; Barycki, J. J.; Simpson, M. A. Emerging roles for hyaluronidase in cancer metastasis and therapy. *Advances in Cancer Research* **2014**, *123*, 1-34. DOI: 10.1016/B978-0-12-800092-2.00001-0.
(34) Karalis, T. Targeting Hyaluronan Synthesis in Cancer: A Road Less Travelled. *Biologics* **2023**, *3* (4), 402-414. DOI: 10.3390/biologics3040022.
(35) Buhren, B. A.; Schrumpf, H.; Gorges, K.; Reiners, O.; Bolke, E.; Fischer, J. W.; Homey, B.; Gerber, P. A. Dose- and time-dependent effects of hyaluronidase on structural cells and the extracellular matrix of the skin. *European Journal of Medical Research* **2020**, *25* (1), 60. DOI: 10.1186/s40001-020-00460-z.
(36) Yoshida, S.; Tomokiyo, A.; Hasegawa, D.; Hamano, S.; Sugii, H.; Maeda, H. Insight into the Role of Dental Pulp Stem Cells in Regenerative Therapy. *Biology* **2020**, *9* (7), 160. DOI: 10.3390/biology9070160.
(37) Hu, B.; Ma, Y.; Yang, Y.; Zhang, L.; Han, H.; Chen, J. CD44 promotes cell proliferation in non-small cell lung cancer. *Oncology Letters* **2018**, *15* (4), 5627-5633. DOI: 10.3892/ol.2018.8051.
(38) Huerta-Angeles, G.; Šmejkalová, D.; Chládková, D.; Ehlová, T.; Buffa, R.; Velebný, V. Synthesis of highly substituted amide hyaluronan derivatives with tailored degree of substitution and their crosslinking via click chemistry. *Carbohydrate Polymers* **2011**, *84* (4), 1293-1300. DOI: 10.1016/j.carbpol.2011.01.021.
(39) Oudshoorn, M. H. M.; Rissmann, R.; Bouwstra, J. A.; Hennink, W. E. Synthesis of methacrylated hyaluronic acid with tailored degree of substitution. *Polymer* **2007**, *48* (7), 1915-1920. DOI: 10.1016/j.polymer.2007.01.068.
(40) Šmejkalová, D.; Hermannová, M.; Šuláková, R.; Průšová, A.; Kučerík, J.; Velebný, V. Structural and conformational differences of acylated hyaluronan modified in protic and aprotic solvent system. *Carbohydrate Polymers* **2012**, *87* (2), 1460-1466. DOI: 10.1016/j.carbpol.2011.09.057.
(41) Pramanik, S. K.; Seneca, S.; Peters, M.; D'Olieslaeger, L.; Reekmans, G.; Vanderzande, D.; Adriaensens, P.; Ethirajan, A. Morphology-dependent pH-responsive release of hydrophilic payloads using biodegradable nanocarriers. *RSC Advances* **2018**, *8* (64), 36869-36878. DOI: 10.1039/c8ra07066k.
(42) Pramanik, S. K.; Pal, U.; Choudhary, P.; Singh, H.; Reiter, R. J.; Ethirajan, A.; Swarnakar, S.; Das, A. Stimuli-Responsive Nanocapsules for the Spatiotemporal Release of Melatonin: Protection against Gastric Inflammation. *ACS Applied Bio Materials* **2019**, *2* (12), 5218-5226. DOI: 10.1021/acsabm.9b00236.
(43) Tiwari, R.; Banerjee, S.; Tyde, D.; Saha, K. D.; Ethirajan, A.; Mukherjee, N.; Chattopadhy, S.; Pramanik, S. K.; Das, A. Redox-Responsive Nanocapsules for the Spatiotemporal Release of

Miltefosine in Lysosome: Protection against Leishmania. *Bioconjugate Chemistry* **2021**, *32* (2), 245-253. DOI: 10.1021/acs.bioconjchem.0c00667.
(44) Mens, R.; Adriaensens, P.; Lutsen, L.; Swinnen, A.; Bertho, S.; Ruttens, B.; D'Haen, J.; Manca, J.; Cleij, T.; Vanderzande, D.; Gelan, J. NMR study of the nanomorphology in thin films of polymer blends used in organic PV devices: MDMO-PPV/PCBM. *Journal of Polymer Science Part A: Polymer Chemistry* **2007**, *46* (1), 138-145. DOI: 10.1002/pola.22365.
(45) Hilkens, P.; Fanton, Y.; Martens, W.; Gervois, P.; Struys, T.; Politis, C.; Lambrichts, I.; Bronckaers, A. Pro-angiogenic impact of dental stem cells in vitro and in vivo. *Stem Cell Research* **2014**, *12* (3), 778-790. DOI: 10.1016/j.scr.2014.03.008.
46) *Biological Evaluation of Medical Devices. Part 5: Tests for In Vitro Cytotoxicity*. ISO 10993-5. International Organization for Standardization, Geneva, Switzerland, **2009**. https://www.iso.org/standard/36406.html.
(47) Lopez-Garcia, J.; Lehocky, M.; Humpolicek, P.; Saha, P. HaCaT Keratinocytes Response on Antimicrobial Atelocollagen Substrates: Extent of Cytotoxicity, Cell Viability and Proliferation. *Journal of Functional Biomaterials* **2014**, *5* (2), 43-57. DOI: 10.3390/jfb5020043.
(48) Lebreton, V.; Legeay, S.; Vasylaki, A.; Lagarce, F.; Saulnier, P. Protein corona formation on lipidic nanocapsules: Influence of the interfacial PEG repartition. *European Journal of Pharmaceutical Sciences* **2023**, *189*, 106537. DOI: 10.1016/j.ejps.2023.106537.
(49) Pancaro, A.; Szymonik, M.; Georgiou, P. G.; Baker, A. N.; Walker, M.; Adriaensens, P.; Hendrix, J.; Gibson, M. I.; Nelissen, I. The polymeric glyco-linker controls the signal outputs for plasmonic gold nanorod biosensors due to biocorona formation. *Nanoscale* **2021**, *13* (24), 10837-10848. DOI: 10.1039/d1nr01548f.
(50) Lu, F.; Luo, Y.; Li, B.; Zhao, Q.; Schork, F. J. Synthesis of Thermo-Sensitive Nanocapsules via Inverse Miniemulsion Polymerization Using a PEO−RAFT Agent. *Macromolecules* **2009**, *43* (1), 568-571. DOI: 10.1021/ma902058b.
(51) Taheri, S.; Baier, G.; Majewski, P.; Barton, M.; Forch, R.; Landfester, K.; Vasilev, K. Synthesis and antibacterial properties of a hybrid of silver-potato starch nanocapsules by miniemulsion/polyaddition polymerization. *Journal of Materials Chemistry B* **2014**, *2* (13), 1838-1845. DOI: 10.1039/c3tb21690j.
(52) Bernardini, J.; Licursi, D.; Anguillesi, I.; Cinelli, P.; Coltelli, M.-B.; Antonetti, C.; Raspolli Galletti, A. M.; Lazzeri, A. Exploitation of Arundo donax L. Hydrolysis Residue for the Green Synthesis of Flexible Polyurethane Foams. *BioResources* **2017**, *12* (2), 3630-3655. DOI: 10.15376/biores.12.2.3630-3655.
(53) Yasarawan, N.; van Duijneveldt, J. S. Arrested phase separation of colloidal rod–sphere mixtures. *Soft Matter* **2010**, *6* (2), 353-362. DOI: 10.1039/b915886c.
(54) Jana, S.; Samanta, D.; Fahad, M. M.; Jaisankar, S. N.; Kim, H. Blocking and Deblocking of Diisocyanate to Synthesize Polyurethanes. *Polymers* **2021**, *13* (17), 2875. DOI: 10.3390/polym13172875.
(55) Rampratap, P.; Lasorsa, A.; Perrone, B.; van der Wel, P. C. A.; Walvoort, M. T. C. Production of isotopically enriched high molecular weight hyaluronic acid and characterization by solid-state NMR. *Carbohydrate Polymers* **2023**, *316*, 121063. DOI: 10.1016/j.carbpol.2023.121063.
(56) Grosu, I. G.; Mot, A.; Filip, X.; Filip, C. What Is Wrong with Hyaluronic Acid Chemistry? A (15)N/(13)C Solid-State NMR Re-Evaluation of Its Dopamine Conjugates. *Polymers* **2023**, *15* (13), 2825. DOI: 10.3390/polym15132825.

(57) Kim, S. W.; Oh, K. T.; Youn, Y. S.; Lee, E. S. Hyaluronated nanoparticles with pH- and enzyme-responsive drug release properties. *Colloids and Surfaces B: Biointerfaces* **2014**, *116*, 359-364. DOI: 10.1016/j.colsurfb.2014.01.017.
(58) Xu, J.; Chen, S.; Yang, J.; Nie, Z.; He, J.; Zhao, Y.; Liu, X.; Zhang, J.; Zhao, Y. Hyaluronidase-trigger nanocarriers for targeted delivery of anti-liver cancer compound. *RSC Advances* **2023**, *13* (16), 11160-11170. DOI: 10.1039/d3ra00693j.
(59) Atashi, F.; Modarressi, A.; Pepper, M. S. The role of reactive oxygen species in mesenchymal stem cell adipogenic and osteogenic differentiation: a review. *Stem Cells and Development* **2015**, *24* (10), 1150-1163. DOI: 10.1089/scd.2014.0484.
(60) Lian, D.; Chen, M. M.; Wu, H.; Deng, S.; Hu, X. The Role of Oxidative Stress in Skeletal Muscle Myogenesis and Muscle Disease. *Antioxidants* **2022**, *11* (4), 755. DOI: 10.3390/antiox11040755.
(61) Wu, G.; Fang, Y. Z.; Yang, S.; Lupton, J. R.; Turner, N. D. Glutathione metabolism and its implications for health. *The Journal of Nutrition* **2004**, *134* (3), 489-492. DOI: 10.1093/jn/134.3.489.
(62) Fasiku, V. O.; Omolo, C. A.; Kiruri, L. W.; Devnarain, N.; Faya, M.; Mocktar, C.; Govender, T. A hyaluronic acid-based nanogel for the co-delivery of nitric oxide (NO) and a novel antimicrobial peptide (AMP) against bacterial biofilms. *International Journal of Biological Macromolecules* **2022**, *206*, 381-397. DOI: 10.1016/j.ijbiomac.2022.02.099.
(63) Sunitha, K.; Suresh, P.; Santhosh, M. S.; Hemshekhar, M.; Thushara, R. M.; Marathe, G. K.; Thirunavukkarasu, C.; Kemparaju, K.; Kumar, M. S.; Girish, K. S. Inhibition of hyaluronidase by N-acetyl cysteine and glutathione: role of thiol group in hyaluronan protection. *International Journal of Biological Macromolecules* **2013**, *55*, 39-46. DOI: 10.1016/j.ijbiomac.2012.12.047.
(64) Berrecoso, G.; Crecente-Campo, J.; Alonso, M. J. Unveiling the pitfalls of the protein corona of polymeric drug nanocarriers. *Drug Delivery and Translational Research* **2020**, *10* (3), 730-750. DOI: 10.1007/s13346-020-00745-0.
(65) Calzada, V.; Cerecetto, H.; Tosar, J. P. *Biotherapeutics: From small to large molecules and cells*, 1st ed.; Topics in Medicinal Chemistry, 42; Springer **2024**. DOI: 10.1007/978-3-031-81025-1.
(66) Raghupathi, K.; Eron, S. J.; Anson, F.; Hardy, J. A.; Thayumanavan, S. Utilizing Inverse Emulsion Polymerization To Generate Responsive Nanogels for Cytosolic Protein Delivery. *Molecular Pharmaceutics* **2017**, *14* (12), 4515-4524. DOI: 10.1021/acs.molpharmaceut.7b00643.

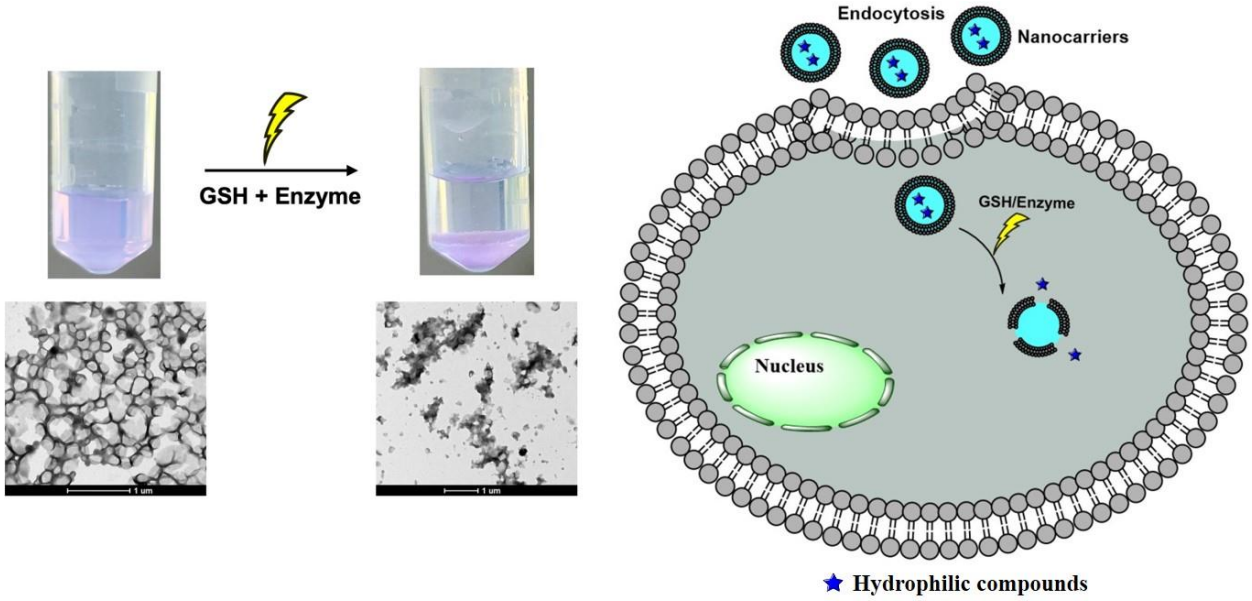

Graphical abstract